Neurobiology of Disease

Chondroitin Sulfate Proteoglycans Potently Inhibit Invasion and Serve as a Central Organizer of the Brain Tumor Microenvironment

Daniel J. Silver,[1] Florian A. Siebzehnrubl,[1] Michela J. Schildts,[1] Anthony T. Yachnis,[2] George M. Smith,[3] Amy A. Smith,[4] Bjorn Scheffler,[5] Brent A. Reynolds,[1] Jerry Silver,[6] and Dennis A. Steindler[1]

[1]Department of Neurological Surgery, University of Florida, Gainesville, Florida 32611, [2]Department of Pathology, Immunology and Laboratory Medicine, University of Florida College of Medicine, Gainesville, Florida 32610, [3]Department of Neuroscience, Temple University, Philadelphia, Pennsylvania 19140, [4]Arnold Palmer Hospital for Children, MD Anderson Cancer Center, Orlando, Florida 32806, [5]Institute of Reconstructive Neurobiology, University of Bonn Medical Center, D-53105 Bonn, Germany, and [6]Department of Neurosciences, Case Western Reserve University, Cleveland, Ohio 44106

Glioblastoma (GBM) remains the most pervasive and lethal of all brain malignancies. One factor that contributes to this poor prognosis is the highly invasive character of the tumor. GBM is characterized by microscopic infiltration of tumor cells throughout the brain, whereas non-neural metastases, as well as select lower grade gliomas, develop as self-contained and clearly delineated lesions. Illustrated by rodent xenograft tumor models as well as pathological human patient specimens, we present evidence that one fundamental switch between these two distinct pathologies–invasion and noninvasion–is mediated through the tumor extracellular matrix. Specifically, noninvasive lesions are associated with a rich matrix containing substantial amounts of glycosylated chondroitin sulfate proteoglycans (CSPGs), whereas glycosylated CSPGs are essentially absent from diffusely infiltrating tumors. CSPGs, acting as central organizers of the tumor microenvironment, dramatically influence resident reactive astrocytes, inducing their exodus from the tumor mass and the resultant encapsulation of noninvasive lesions. Additionally, CSPGs induce activation of tumor-associated microglia. We demonstrate that the astrogliotic capsule can directly inhibit tumor invasion, and its absence from GBM presents an environment favorable to diffuse infiltration. We also identify the leukocyte common antigen-related phosphatase receptor (*PTPRF*) as a putative intermediary between extracellular glycosylated CSPGs and noninvasive tumor cells. In all, we present CSPGs as critical regulators of brain tumor histopathology and help to clarify the role of the tumor microenvironment in brain tumor invasion.

Introduction

Diffuse infiltration of tumor cells throughout the brain is a central hallmark of high-grade astrocytomas [such as glioblastoma (GBM), World Health Organization (WHO) grade IV astrocytoma; Furnari et al., 2007; Louis et al., 2007]. In the most severe cases, microscopic insinuation of the tumor involves large portions of the brain, spreading bilaterally across both hemispheres (DeAngelis, 2001). In contrast, certain lower grade gliomas as well as non-neural metastases tend to form expanding, but discrete, noninvasive lesions. The biological determinants of these two distinct behaviors remain unclear. We are beginning to appreciate that interplay between tumor cells and their surrounding environment can facilitate (Markovic et al., 2009; Edwards et al., 2011), or possibly deter invasion, but the medium through which this exchange occurs remains largely unexplored. The tumor extracellular matrix (ECM) is physically positioned at the junction between the tumor and its microenvironment, and as such, may be uniquely situated to serve as a critical regulator of these interactions.

Chondroitin sulfate proteoglycans (CSPGs) are a diverse family of ECM molecules. Each family member consists of a core protein, for which it is named, covalently linked to at least one, long chain chondroitin sulfate glycosaminoglycan (CS-GAG) polysaccharide (Galtrey and Fawcett, 2007). During CNS development, glycosylated CSPGs are expressed in specific locations and are thought to serve as molecular barriers, constraining cells against movement across the boundary of two adjacent, emerging structures (Cooper and Steindler, 1986; Steindler et al., 1988; Snow et al., 1990; Brittis et al., 1992; Jhaveri, 1993; Faissner and

Received June 25, 2012; revised July 29, 2013; accepted Aug. 23, 2013.

Author contributions: D.J.S., F.A.S., B.A.R., J.S., and D.A.S. designed research; D.J.S. and M.J.S. performed research; A.T.Y., G.M.S., A.A.S., and B.S. contributed unpublished reagents/analytic tools; D.J.S. and F.A.S. analyzed data; D.J.S., F.A.S., B.A.R., J.S., and D.A.S. wrote the paper.

Financial support was provided by the Maren, Thompson, and McKinney Regeneration funds, and National Institutes of Health grants NS055165 (D.A.S.) and 5T32DK074367–02 (D.J.S. training grant). We thank the University of Florida Department of Neurosurgery and Barbara Frentzen of the Florida Center for Brain Tumor Research for providing human tumor specimens. We also thank Dr. Lung-Ji Chang for his guidance with lentiviral transduction, Marda Jorgensen for her technical assistance with human tissue preparation and IHC, Dr. David Muir for his assistance with dot-blot analysis, and Philip Carlson for graphic illustration. Drs. Loic Deleyrolle, Matthew Sarkisian, and David Borchelt offered keen insights and critical reviews of this manuscript. We are indebted to the Lockwood, Barajas, Larkin, and Wohrle families, as well as the Rock by the Sea and the Noah's Light Foundations for their generosity and support.

The authors declare no competing financial interests.

This article is freely available online through the *J Neurosci* Author Open Choice option.

Correspondence should be addressed to Daniel J. Silver, Human Biology Division, Fred Hutchinson Cancer Research Center, 1100 Fairview Ave North, Seattle, WA 98109. E-mail: dsilver@fhcrc.org.

DOI:10.1523/JNEUROSCI.3004-12.2013

 0270-6474/13/3315603-15$15.00/0

Steindler, 1995; Heyman et al., 1995; Golding et al., 1999). Additionally, injuries to the CNS (Silver and Miller, 2004) as well as the rare sites of neurogenesis in the adult mammalian brain are spatially defined and isolated from surrounding structures by abundant glycosylated CSPGs (Gates et al., 1995; Thomas et al., 1996; Akita et al., 2008; Silver and Steindler, 2009). These inhibitory/repulsive properties are mediated largely through the numerous sulfated CS-GAG side chains tethered to the CSPG core proteins. Interestingly, CSPGs associated with invasive brain tumors are thought to promote, rather than restrict tumor cell invasion (Jaworski et al., 1996; Zhang et al., 1998; Müller et al., 2003; Viapiano et al., 2005; Arslan et al., 2007; Varga et al., 2012). In these cases, however, most investigators have not differentiated between the CSPG core proteins and their covalently linked CS-GAGs. Thus, the inhibitory properties of the sugar side chains have not been fully addressed in the context of the brain tumor microenvironment or the invasive niche.

Here, we study noninvasive and diffusely invasive brain tumors with a specific emphasis on glycosylated CSPGs and their contributions to the overall tumor microenvironment. We have focused on clarifying the ways in which tumor cells interact with the ECM and the effects that tumor-derived CSPGs have on resident, reactive astrocytes and microglia. In total, we present novel insights into the interconnectivity of tumor cells, the ECM, and resident glia and help to explain how the microenvironment can either permit or inhibit tumor cell invasion.

Materials and Methods

Cell culture

Primary human cancer cell culture. *h*GBM L0 (43 year old male) and *h*GBM L1 (45 year old female) were initially described by Galli et al. (2004) and Deleyrolle et al., (2011), respectively. *h*GBM L19 (9 year old male) and *h*Glioma Grade II L7 (54 year old female) were derived under the following adherent conditions: the specimen was initially subdivided into multiple 1 mm^3 micro-explants and distributed evenly within a minimal volume of N2 growth medium supplemented with fetal bovine serum (FBS; 5%, Atlanta Biologicals), epidermal growth factor (*rh*EGF 10 ng/ml; R&D Systems), fibroblast growth factor (*rh*FGF-basic, 10 ng/ml; R&D Systems), leukemia inhibitory factor (*rh*LIF, 1 μl/ml; Millipore), and natural mouse laminin (1 μl/ml; Invitrogen). For 7–10 d, the media volume was gradually increased while tumor-derived cells began to emigrate from the micro-explants and proliferate. The tissue fragments were finally discarded and the growth medium was exchanged. Complete medium, including mitogens and laminin, was exchanged every other day until the culture reached 85–90% confluence. The cells were then culled and cryopreserved for future use in these studies.

During the course of these studies, primary human cancer cell lines were propagated under the following adherent culture conditions. A single-cell suspension of 50,000 cells/ml in N2 growth medium, supplemented by FBS (5%), *rh*EGF, and *rh*FGF (10 ng/ml each) was seeded onto a poly-L-ornithine (15 μg/ml)-coated culture surface. Medium and supplements were exchanged every other day until the cultures reached 85–90% confluence. Cultures were passaged weekly using trypsin-EDTA (0.25% trypsin, 1 mM EDTA; Atlanta Biologicals) and filtered through a 70 μm cell strainer (BD Biosciences) before replating.

Classic human cancer cell culture. U-87MG (ATCC) was propagated in Minimum Essential Eagle Medium (EMEM, ATCC) supplemented with 10% fetal calf serum (FCS) according to standard protocols with the following modification. Between each passage, cells were strained through a 70 μm mesh before reseeding at 50,000 cells/ml in complete growth medium.

Primary murine astrocyte cell culture. Murine astrocytes were derived as described previously (Scheffler et al., 2005). Briefly, a block of tissue containing the lateral ventricles, septum, and bilateral striata was prepared from 4- to 8-d-old C57BL/6J mice. Enzymatic and subsequent mechanical dissociations yielded a single-cell suspension comprised of ≥95% $GFAP^+$ astrocytes. Cells were plated in N2 medium containing 5% FBS, *rh*EGF, and *rh*FGF (10 ng/ml, each). Growth medium was exchanged every other day until the cultures reached 85–90% confluence. Cultures were passaged weekly using trypsin-EDTA and filtered through a 70 μm cell strainer before reseeding at 50,000 cells/ml in complete growth medium.

Primary murine microglial cell culture. Microglia were isolated from established astrocyte monolayers according to Marshall et al. (2008). Briefly, primary or first passage astrocyte cultures were grown to 100% confluence. Standard N2 growth medium was then replaced with a reformulated N2 growth medium supplemented with 10% FCS and GM-CSF (20 ng/ml; Stem Cell Technologies). This modified growth media was exchanged every other day for 5–7 d, during which, phase-bright, spherical microglia gradually accumulated. At week's end, the culture flask was gently agitated at room temperature for 15–30 min to loosen the microglial cells that were directly attached to the astrocyte monolayer. The detached microglia were then collected for further experimentation.

Genetic modification of cancer cell lines

U-87MG cells were transduced with lentiviral vectors encoding the genes for either chondroitinase ABC (LV-Ch'ase ABC; courtesy of Dr. G. Smith, Temple University, Philadelphia, PA) or enhanced green fluorescent protein (LV-*e*GFP; generously provided by Dr. L. Chang, University of Florida, Gainesville, FL). Additionally, *h*GBM L19 cells were transduced with a lentiviral vector encoding the gene for firefly luciferase (LV-*f*Luc; generously provided by Dr. L. Chang). Cells (50,000 cells/ml) were plated into a 6-well plate. After a brief attachment period, the medium was exchanged with a minimal volume (500 μl/well) of complete growth medium, containing polybrene (10 μg/ml; Sigma) and virus. One well was reserved as a nontransduced, negative control, and a second was used to control for the polybrene. The other four received progressively increasing viral titers, from 10 to 100 multiplicity of infection (MOI). Media was exchanged with standard growth medium 36 h later and every other day thereafter until the cultures reached 85–90% confluence. The single well of transduced cells with the highest MOI that demonstrated a growth rate equivalent to the nontransduced control was carried forward and expanded for subsequent experimentation.

CSPG–laminin spot gradient assay

The spot assay was adapted from Tom et al. (2004). Briefly, spots were prepared by placing four, 3 μl droplets of DMEM/F12 containing mixed CSPGs (10–500 μg/ml; Millipore) and laminin (5 μg/ml; Invitrogen) onto poly-L-ornithine (15 μg/ml) and nitrocellulose pretreated glass coverslips and allowed to dry completely. Additionally, negative control spots consisting of bovine serum albumin (BSA: 25–500 μg/ml; Sigma) and laminin (5 μg/ml) as well as laminin-alone (5 μg/ml) were prepared in parallel with the experimental groups. The entire coverslip was then suffused with a solution of laminin (5 μg/ml) in DMEM/F12 and incubated at 37°C for at least 3 h. The laminin solution was aspirated immediately before plating 50,000 primary murine astrocytes suspended in standard astrocyte growth medium. Media was exchanged every other day until the culture reached 85–90% confluence within the nonspotted portion of the cover glass. The completed assay was then fixed with 4% formaldehyde and immunostained for vimentin, CS-56, and laminin (Table 1). For the invasive/noninvasive coculture spot assays, spots were prepared using 500 μg/ml CSPGs and 5 μg/ml laminin and performed in parallel. Before astrocyte plating, the invasive phenotype spots were treated extensively with Ch'ase ABC (1U/ml; AMS Biotechnology) for 3 d, exchanging the Ch'ase ABC-containing media each day. Primary murine astrocytes (50,000), suspended in standard astrocyte growth medium, were then plated evenly across the coverslips. Media was exchanged every other day until the cultures reached 50–75% confluence within the nonspotted portion of the cover glass. The noninvasive phenotype spots then received a rapid Ch'ase ABC treatment (1U/ml; 3–5 h, 37°C) sufficient to reduce the CS-GAG content of the spots while preserving the astrocyte circumscription. *h*GBM L1 cells (80,000) were then plated uniformly across all coverslips. Media was exchanged every other day until the astrocytes reached 95–100% confluence within the non-

Table 1. Vendor and dilution information for all primary antibodies used in this study

Antigen	Host species	Dilution	Vendor	Catalog no.
Human Nestin	Rabbit	1/1000	Millipore	AB5922
Human Nestin	Mouse	1/1000	Millipore	MAB5326
*e*GFP	Chicken	1/1000	Aves Labs	GFP-1020
Firefly luciferase	Rabbit	1/200	Abcam	ab21176
GFAP	Rabbit	1/400	Dako	Z0334
Vimentin	Rabbit	1/500	Epitomics	2707-1
β-III tubulin	Mouse	1/1000	Promega	G712A
Iba1	Rabbit	1/500	Wako	019-19747
CD11b	Rat	1/200	BD Pharmingen	550282
ED-1	Rat	1/200	Abcam	ab53444
LAR	Mouse	1/250	BD Biosciences	610350
PTPσ	Goat	5 μg/ml	R&D Systems	AF3430
NogoR	Rabbit	1/500	Abcam	ab26291
Laminin	Rabbit	1/2000	Biomedical Technologies	BT-594
Biotinylated-WFA lectin		1/500	Vector Laboratories	B-1355
CS-56	Mouse	1/200	Sigma	C8035
DSD-1	Rat	1/1000	Millipore	MAB5790
C-4-S	Mouse	1/500	Millipore	MAB2030
C-6-S	Mouse	1/500	Millipore	MAB2035
2-B-6	Mouse	1/1000	MD Biosciences	1042009
ACAN	Mouse	1/500	Millipore	MAB5284
BCAN	Sheep	1/500	R&D Systems	AF4009
NCAN	Rabbit	1/250	Epitomics	5452-1
PCAN	Mouse	1/500	BD Biosciences	610180
VCAN	Mouse	1/1000	DSHB	12C5-s
β-actin	Mouse	1/5000	Abcam	ab6276

spotted portion of the cover glass before formaldehyde fixation and immunocytochemistry. The cover glasses were mounted to slides and examined using a Leica DMLB standard fluorescent microscope. To quantify the astrocyte spot assays (see Fig. 3), six evenly spaced images were captured around the rim of each spot at 100× magnification. The total number of astrocytes with DAPI$^+$ nuclei in the outer-spot region, which extended processes across the rim of the spot, were tallied using the ImageJ Cell Counter plug-in (National Institutes of Health, Bethesda, MD). The same ImageJ counting plug-in was used to quantify the invasive/noninvasive coculture spot assays (see Fig. 7); however, in these cases, the total number of *h*Nestin$^+$ cells beyond the outer rim of the spots was tallied and compared.

Protein isolation, Western, and dot-blot analysis

Proteins were isolated from cancer cell cultures and xenografted tumor specimens as described previously (Siebzehnrubl et al., 2013). For Western blotting, 15 μg of denatured protein was loaded on 4–12% Bis-Tris reducing gels (Invitrogen), electrophoresed, and blotted onto PVDF membranes (iBlot; Invitrogen). Blots were blocked with 5% nonfat milk in Tris-buffered saline containing 0.1% Tween 20, probed with primary (Table 1) and appropriate horseradish peroxidase-conjugated secondary antibodies, and developed using the Pierce ECL Plus kit (Thermo Scientific) on a FluorChem Q Multi Image III Imaging center (Cell Biosciences) equipped with Alpha Innotech software version 1.0.1.1. For dot blots, 5–50 μg of native protein was blotted onto 0.45 μm nitrocellulose membranes (Bio-Rad) using the Bio-Rad, Bio-Dot Apparatus and processed as described above for Western blots. To identify CSPG neo-epitopes, protein lysates were pretreated with Ch'ase ABC (1U/ml; overnight, 37°C) before blotting.

Microglial activation assay

Rather than discrete spots, microglial activation was assayed on evenly coated glass coverslips using the same concentrations of poly-L-ornithine, laminin, and CSPGs as used in the spot assay. Negative control coverslips coated with BSA and laminin as well as laminin alone were prepared in parallel with the experimental groups. After 3 h, the laminin/CSPG solutions were aspirated and replaced by 50,000 primary murine microglia in microglial proliferation medium. Media was exchanged every other day for 5 d before fixation with 4% formaldehyde. The completed assay was immunostained for CD11*b* (Table 1). The cover glasses were mounted to slides and surveyed at 100× magnification by a blinded observer (M.J.S.) in a series of 10 nonoverlapping images. Each cell was scored as either ramified or activated based on its unique morphology. For these purposes, "ramified" microglia were defined by a complex structure with three or more elaborate peripheral extensions. In comparison, "activated" microglia were essentially spherical, simple cells without elaborate processes. A subset of microglia presented a morphology that was difficult to classify. These so-called "pseudoramified" cells fell between the extremes of microglial activation and rest. These partially activated cells were designated as activated to maintain the objectivity of the scoring system.

In vitro tumor dispersal assay

U-87MG tumor cells (50,000 cells/ml) were plated into an untreated, 6-well plate in standard growth media. Immediately thereafter, either Ch'ase ABC (0.025–0.1 U/ml) or the negative control enzyme penicillinase (0.025–0.1 U/ml) was added to the culture media. Complete growth media, including enzyme, was exchanged every other day to compensate for the thermolability of Ch'ase ABC at 37°C. Cultures were maintained until the 0.1 U/ml Ch'ase ABC-treated wells reached 85–90% confluence. Using a Leica DM IRB inverted microscope outfitted with a Leica DFC 300F digital camera, the aggregate-occupied area of the growth surface was recorded in a series of two to four, low-magnification (25×) phase contrast images. The Photomerge automation for Photoshop CS4 (Adobe Systems) was then used to reconstruct the entire aggregate-occupied area into a single image. Finally, the total number of phase-dark aggregates was quantified using the ImageJ Cell Counter plug-in.

Intracranial transplantation

Surgical procedures

All animal procedures were conducted in accordance with University of Florida Institutional Animal Care and Use Committee-approved protocols. Adult female NOD/SCID mice (Charles River Laboratories) were anesthetized with inhaled isoflurane (2–2.5%;) and fit to a stereotaxic apparatus. A burr hole was drilled 0.5 mm rostral and 1.8 mm lateral to bregma. A 33 gauge, stainless steel needle (Hamilton) was lowered 2.5 mm beneath the surface of the brain and 50,000 cells suspended in 1 μl of sterile culture medium were slowly injected over ~5 min. The needle was held in place an additional 5 min before removal and closing. It was important that animals were culled before the tumor mass had become so large that the tumor microenvironment could no longer be appreciated. As such, animals transplanted with U-87MG survived no longer than 4 weeks, whereas animals transplanted with the primary *h*GBM cell lines survived up 13 weeks.

Tissue preparation and immunohistochemistry

At the close of the postoperative period, all animals were anesthetized and transcardially perfused with 4% formaldehyde in PBS. The brain was removed and postfixed overnight. The tissue was then cryoprotected with sequential treatments in solutions of 30% sucrose (Sigma) and 1:1 30% sucrose: O.C.T. Compound (Tissue-Tek). Finally, the tissue was embedded in O.C.T. Compound and 20 μm coronal sections were prepared for subsequent immunohistochemical analysis using standard protocols. A detailed list of the antibodies used can be found in Table 1. In all cases, primary antibodies were coupled to appropriate Alexa Fluor 488, or 555, or Pacific Blue-conjugated secondary antibodies.

Quantification of in vivo *tumor invasion*

Engrafted human glioma cells were detected using an antibody raised against human-specific Nestin. Additionally, for context, the host tissue was stained with an antibody raised against β-III tubulin and nuclei were visualized with DAPI (0.1 μg/ml; Sigma). The stained sections were mounted onto slides, coverslipped, and examined using a Leica DMLB epifluorescence microscope equipped with a Spot RT3 CCD camera (Diagnostic Instruments). Using Spot Advanced software (Diagnostic Instruments) the tumor-bearing hemisphere was recorded in a series of

50× magnification images. The Photomerge automation for Photoshop CS4 was then used to reconstruct the entire series into a single image. Inverting the image into a black-on-white image isolated the tumor and the threshold was adjusted to distinguish the tumor from any nonspecific background staining. Finally, the ImageJ Analyze Particles function was used to quantify the total number of discrete particles contained within the tumor. We found that diffusely invasive tumors were made up of several thousand times (~2000–7300) more discrete, noncontiguous particles than noninvasive lesions.

Human tissue collection and processing

All human tissue was acquired and processed in accordance with University of Florida Institutional Review Board-approved protocols. Briefly, 5 μm thin sections were prepared from de-identified blocks of paraffin-embedded human tumor specimens, obtained from the University of Florida Department of Neuropathology. The slides were sequentially de-paraffinized, rehydrated, and blocked for endogenous peroxidase activity. Optimal staining required 25 min of antigen retrieval in 10 mM citrate buffer (pH 6.0). The tissue was then immunostained at 4°C, overnight for the antigens CS-56 and GFAP (Table 1). Slides were stained using the ABC-Elite kit (Vector Laboratories) following the manufacturer's instructions, with endogenous biotin-blocking steps included. Positive staining was detected with diaminobenzidine (Vector Laboratories) as the chromogen and hematoxylin 560 (SurgiPath) as the nuclear counterstain.

Statistical analysis

Data were analyzed with GraphPad Prism 5.0 (GraphPad Software) software package. In all cases, a p value of <0.05 was deemed significant.

Results

Self-contained, focused lesions, but not diffusely invasive brain tumors are associated with the robust expression of CS-GAGs

Immune-compromised, NOD/SCID mice received intrastriatal transplants from five human glioma cell lines: U-87MG, *h*Glioma Grade II L7, *h*GBM L0, *h*GBML1, and *h*GBML19 ($n \geq 6$ each). Immunohistological examination revealed extensive dissemination of the primary *h*GBM cells throughout the transplanted brain (Fig. 1*A*), which contrasted sharply with the focused, noninvasive lesions generated by U-87MG and *h*Glioma Grade II L7 (Fig. 1*B*). Immunostaining for human nestin (*h*Nestin), which labels the engrafted human tumor cells and excludes any rodent host cells, revealed that the three primary glioblastoma cell lines (*h*GBM L0, *h*GBM L1, and *h*GBM L19) produced diffusely infiltrating tumors. In these cases, there was no discernable edge to the primary tumor mass. Rather, the tumor gradually faded, at a microscopic level into the surrounding tissue (Fig. 1*C–E*). Given time, each of these cell lines demonstrated long-distance invasion, most commonly along myelinated fiber tracts, involving both the initially transplanted and contralateral hemispheres. Conversely, tumors generated from U-87MG and *h*Glioma Grade II L7 presented as focused masses of cells with clear, well defined edges (Fig. 1*F*,*G*). In contrast to the uniform tumors derived from U-87MG, *h*Glioma Grade II L7 generated irregularly shaped lesions with undulating outer edges. However, no tumor cells were observed beyond the outer boundaries of either noninvasive tumor type. Conversion of the fluorescent *h*Nestin immune reactions into black and white threshold images (Fig. 1*H–L*) highlighted the matching patterns of infiltration observed by the invasive tumor cells and punctuated the significant differences in invasion between invasive and noninvasive tumors (Fig. 1*M*). Because the extent of invasion is a function of time, it is important to note that invasion was assessed at different time points (4–6 weeks for U-87MG, *h*Glioma Grade II L7, and *h*GBM L19; 10 weeks for *h*GBM L0; and 13 weeks for *h*GBM L1), which allowed for the various growth rates of each individual patient-derived tumor line. Invasion was quantified once the developing tumors (at minimum) occupied the same proportion of the transplanted striata. It is important to note that in our experience, which coincides with classic clinical observations (Scherer, 1940), time was not a factor in determining whether a tumor would invade or not. During our initial testing of each of these lines, in accordance with findings presented by Sampetrean et al. (2011), even at the earliest time points examined, invasive tumors presented as infiltrating lesions and noninvasive tumors presented as self-contained masses of cells.

Further investigation into the microenvironment of these different tumor types revealed striking differences in the composition of the ECM. Immunohistochemical staining for CS-polysaccharide side chains with WFA-Lectin and the CS-56 antibody revealed that noninvasive tumors were associated with an intense expression of glycosylated CSPGs within the immediate tumor microenvironment. The proteoglycan precisely defined the tumor mass up to and including the sharp edge of the tumor but no further (Fig. 2*A–B″*,*H*; equivalent images of CS-56 immunostaining not shown). Conversely, WFA-Lectin and CS-56 immune reactivity was essentially absent from the invasive tumors (Fig. 2*C–E″*,*H*). Aside from consistent labeling of the perineuronal nets within the cortices and basal ganglia of the transplanted brains (Fig. 2*C′*,*D′*,*E′*) and inconsistent (low-level) expression within the necrotic cores of the primary *h*GBM L0 and *h*GBM L19 tumor masses, CS-GAGs were comparatively absent from the microenvironment of the diffusely invasive tumors (Fig. 2*F*). Importantly, dot-blot analysis of concentrated, conditioned media from cultured glioma cells as well as whole-tumor protein lysates reaffirmed the disparity in glycosylated CSPGs between invasive and noninvasive tumors. Additionally, Ch'ase ABC treatment and subsequent dot-blot analysis confirmed the specificity of our CS-56 and WFA-Lectin staining by revealing the expression of the three CS-neo-epitopes: 2-B-6, C-4-S, and C-6-S (Fig. 2*G*). We also observed the identical staining pattern for the DSD-1 antibody (Fig. 2*H*,*I*,*M*), which binds to a uniquely sulfated CS-GAG and is only poorly detected by CS-56 and WFA-Lectin (Ito et al., 2005). The absence of DSD-1 immunostaining from the invasive tumors ruled out the possibility that the invasive tumors may have switched to a CS-GAG expression profile unrecognized by our labeling methods.

This dichotomy of CS-GAG expression between invasive and noninvasive tumors was especially striking considering the substantial precedent for CSPGs in glioma invasion (Jaworski et al., 1996; Zhang et al., 1998; Müller et al., 2003; Zheng et al., 2004; Arslan et al., 2007; Varga et al., 2012). To address the novel possibility that CSPG core proteins may be differentially glycosylated in invasive versus noninvasive tumors, we surveyed tumors derived from each of the five human glioma cell lines for five CSPG core proteins: aggrecan (ACAN), brevican (BCAN), neurocan (NCAN), versican (VCAN), and phosphacan (PCAN). The results of this survey clarified that both tumor types expressed various CSPG core proteins. Specifically, VCAN, BCAN, NCAN, and PCAN were readily detectable *in vivo* across multiple tumor types, whereas ACAN was only detected in the conditioned media of cultured U-87MG and *h*GBM L19 tumor cells (Fig. 2*H*). *In vivo*, the noninvasive tumors (U-87MG and *h*Glioma Grade II L7) were characterized by their uniform expression of VCAN throughout the mass, up to and including the outer edge of the lesions (Fig. 2*J*). Each of the core proteins expressed by *h*GBM L0- and *h*GBM L1-derived tumors were observed within the

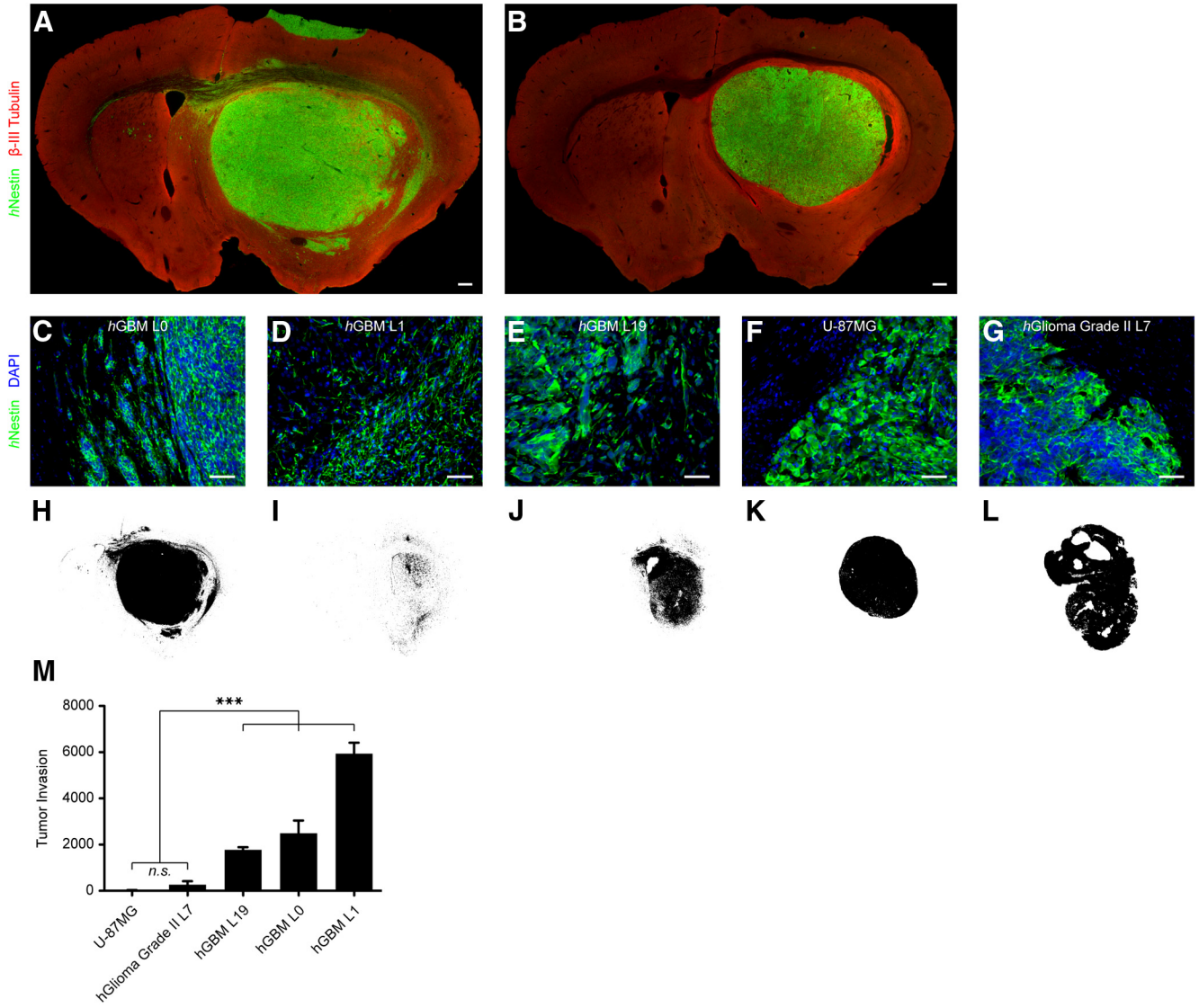

Figure 1. Differential invasion results from transplanting various human glioma cell lines. ***A***, A series of primary human GBM (*h*GBM) cell lines presents the diffusely invasive pathology of high-grade glioma better than (***B***) the conventional xenograft model, U-87MG, or the primary human grade II astrocytoma, *h*Glioma Grade II L7. ***C–E***, Microscopic infiltration is readily observable across each of the primary *h*GBM cell lines (***F–G***) as compared with the noninvasive phenotype typical of engrafted U-87MG and *h*Glioma Grade II L7. ***H–M***, Overall tumor invasion is quantified based on threshold images prepared from tumor-bearing sections of engrafted animals and emphasizes the significant disparities between invasive and noninvasive tumor phenotypes (mean ± SEM, one-way ANOVA, Bonferroni-Dunn *post hoc* test, $^{***}p < 0.0001$ as compared with U-87MG and *h*Glioma Grade II L7, $n = 6$/group).

densest regions of the central tumor core (Fig. 2*N*,*K*,*L*); however, NCAN and PCAN expression extended to the larger tendrils and collectives of invading cells proximal to the tumor mass (Fig. 2*O*,*P*). Core protein expression was not detected at the single, infiltrating tumor cell level for any of the invasive tumors. Curiously, none of the CSPG core proteins or CS-GAGs were detected from *h*GBM L19 *in vivo*. Thus, while both invasive and noninvasive tumors expressed a variety of CSPG core proteins, readily detectable CS-glycosylation was only observed in the noninvasive subtypes.

Tumor-associated CS-GAGs may be sufficient to induce host astrocyte withdrawal to the edge of the tumor mass

Host astrocytes responded differently to invasive and noninvasive brain lesions. Astrocytes were largely absent from the space occupied by noninvasive lesions, but abundant and densely packed into the space immediately beyond their outermost edge (Fig. 3*A*). This resulted in the encapsulation of the noninvasive tumor within multiple layers of highly interwoven astrocytic processes (Fig. 3*B*,*B*′). In contrast, the astrocytes associated with invasive tumors were not physically displaced by the growing tumor (Fig. 3*C*). Although also reactive and hypertrophic, these astrocytes formed elaborate networks of processes throughout the entire tumor, yet by comparison, showed no evidence of displacement or withdrawal away from the tumor mass (Fig. 3*D*,*D*′). It is likely that mass effect contributes to astrogliotic encapsulation; however, physical pressure alone cannot explain the differential astrocyte responses observed. Astrocytes were only displaced by the CS-GAG-expressing noninvasive tumors, even though both the noninvasive as well as the invasive *h*GBM L0 and *h*GBM L19 tumors established dense tumor cores (Fig. 1*H*,*J–L*). Importantly, the central masses of invasive *h*GBM L0 and *h*GBM L19 tumors, where mass effect was presumably greatest, did not physically displace the cohabitant astrocyte population. We reasoned that astrocyte encapsulation might be the result of an active molecular repulsion. Because the tumor ECM

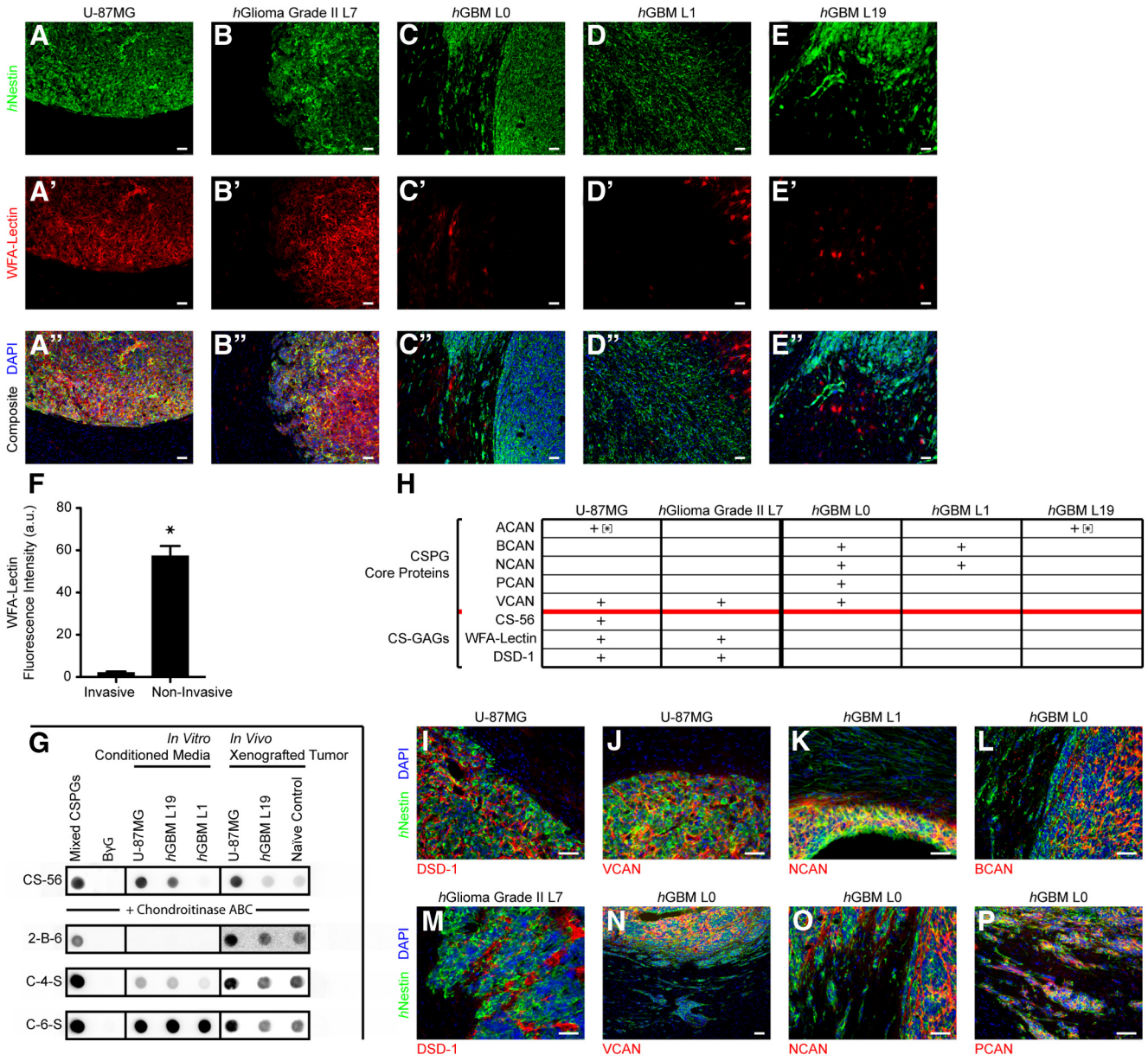

Figure 2. CSPG glycosylation distinguishes noninvasive from invasive glioma. ***A–B″***, CS-GAGs are present in great abundance within the ECM of noninvasive, strictly expansively growing lesions (***C–E″***) whereas diffusely invasive *h*GBM xenografts develop in an environment deplete of glycosylated CSPGs. ***F***, Quantification of the fluorescence intensity of the CS-GAG-binding WFA-Lectin reveals the dissimilarity in CS-glycosylation between invasive and noninvasive glioma *in vivo* (a.u., arbitrary units; mean ± SEM, unpaired *t* test, $*p < 0.0001$, $n = 18$/group). ***G***, Dot-blot analysis of Ch'ase ABC-digested conditioned media from cultured glioma cells or whole-tumor protein lysates confirms the presence of CSPGs by revealing the CS-GAG neo-epitopes 2-B-6, C-4-S, and C-6-S. Additionally, a nominal quantity of glycosylated CSPGs and CS-neo-epitopes was observed within invasive tumors, equal to that in the naive rodent brain. ***H***, Summation of the CS-GAG and CSPG core protein expression profiles of two noninvasive (U-87MG and *h*Glioma Grade II L7) and three invasive (*h*GBM L0, L1, and L19) brain tumor types clarifies a disparity in CSPG glycosylation between infiltrating and noninfiltrating gliomas. ***I–P***, Representative immunophotomicrographs of the data summarized in ***H***. Scale bar, 50 μm.

is so different between these separate tumor types, we hypothesized that the tumor ECM, specifically tumor-associated CS-GAGs, could be one set of factors responsible for the dramatic displacement of astrocytes away from noninvading lesions. We therefore tested whether CS-GAGs, by themselves, could induce astrocyte encapsulation in an adaptation of the *in vitro* spot assay (Tom et al., 2004). The spot assay involves the generation of an inhibitory rim of proteoglycan around the outer edge of a single, circular spot. The growth-permissive protein laminin occupies the center of each spot and gradually tapers off approaching the edge, whereas a mixture of glycosylated CSPGs, including NCAN, PCAN, VCAN, and ACAN, deposits at the edge of the spot and tapers off approaching the center. A uniform coating of laminin is applied to the remaining unspotted growth surface creating a sharp interface between laminin and the CSPG^{High} outermost edge of the spot (Fig. 3*E*, dashed line). We challenged primary, subcortical mouse astrocytes with spots, prepared with progressively greater concentrations of CSPGs. Low concentrations of proteoglycans presented a permissive growth substrate that did not displace cultured astrocytes. Rather, astrocytes grew uniformly across the spotted cover glass except for the outer rim of the spot where astrocytes encountered the highest concentrations of CS-GAGs (Fig. 3*F*). With increasing levels of CSPGs, fewer and fewer astrocytes grew within the inhibitory spot resulting in a progressively cleaner circumscription of the spotted region, analogous to the effect seen around noninvasive tumors

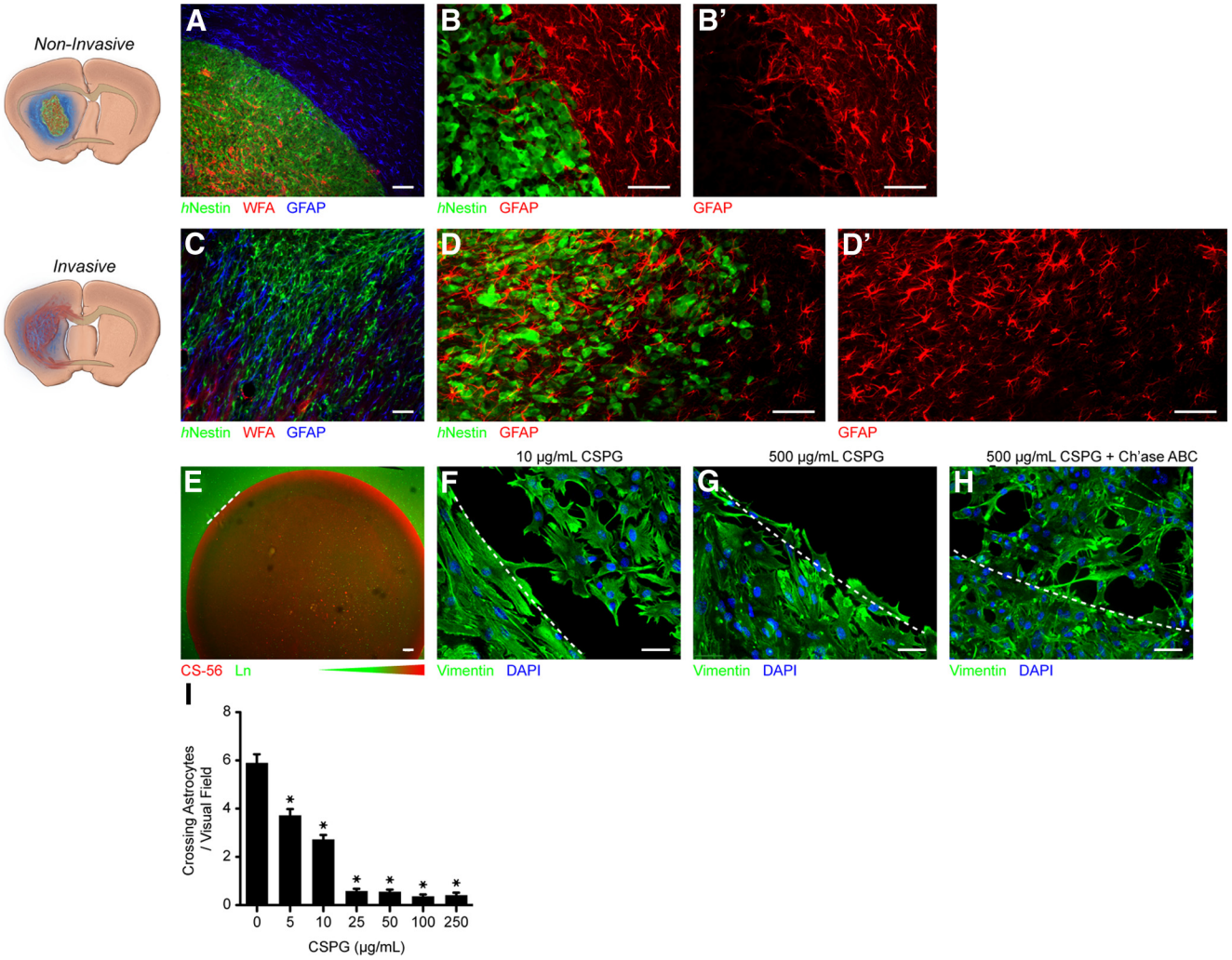

Figure 3. Reactive astrocytes withdraw from the space occupied by CS-GAG-rich noninvasive lesions but persist throughout regions occupied by invasive tumor cells. Representative (***A***) low- and (***B***) high-magnification fluorescence micrographs illustrate the astrocytic encapsulation of noninvasive, CS-GAG-dense lesions. ***B′***, Note the scant GFAP $^{+}$ processes remaining at the very outer limits of the noninvasive mass. ***C–D′***, In contrast, fluorescence micrographs of invasive lesions exemplify widespread occupation by reactive astrocytes. ***E***, Spot-gradient assays generate highly concentrated, CS-GAG-containing regions (area to the right of the dashed line), analogous to the CS-GAG-rich ECM of a noninvasive lesion, and allow us to illustrate the strong aversion that reactive astrocytes have toward CSPGs. ***F***, At low concentrations of CS-GAGs, the spot presents a permissive substrate for astrocyte growth. ***G***, However, with increasing CS-GAG concentration, the spotted region becomes increasingly growth inhibitory, resulting in astrocyte encapsulation of the spot—note the absence of astrocytes in the region to the right of the dashed line. ***H***, Treatment of otherwise potently inhibitory spots with Ch'ase ABC confirms that the growth inhibitory properties of CSPGs derive specifically from their covalently linked CS-GAGs. ***I***, Quantification of the spot-gradient assay emphasizes the inhibitory effects of high levels of CS-GAGs on reactive astrocytes (mean ± SEM, one-way ANOVA, Tukey's *post hoc* test, $^{*}p < 0.0001$ compared with 0, $n = 12$ spots/condition). Scale bar, 50 μm.

(Fig. 3*G*). It was important that we rule out the possibility that the astrocytes might be repelled not by CSPGs, but merely by the growing abundance of protein within the spot. No astrocyte repulsion or circumscription was noted when CSPGs were substituted with equal concentrations of BSA, even at the highest concentrations of total protein (data not shown). Additionally, it was critical that we demonstrate that the astrocyte response resulted specifically from the abundance of CS-GAGs and not CSPG core proteins. The inner portion of spots generated with 500 μg/ml CSPGs were initially completely inhospitable to cultured astrocytes (Fig. 3*G*). By treating these spots with Ch'ase ABC, which maintains the CSPG core proteins while removing all but a stub of the lengthy CS-GAG side chains, the spotted region was converted back into a permissible growth environment (Fig. 3*H*). Thus, these data suggest that abundant CS-GAGs are sufficient to induce astrocyte displacement, and by extension may help explain the astrocyte phenotype surrounding a CS-GAG-enriched, noninvasive tumor.

Microglial activation state distinguishes self-contained, focused lesions from diffusely invasive brain tumors

Unlike astrocytes, microglia uniformly populated both types of brain tumors: invasive and noninvasive (Fig. 4*A*,*D*). Interestingly, however, differences in microglial activation states were immediately apparent. Iba1 immunostaining revealed that microglia associated with invasive brain tumors presented a ramified morphology (Fig. 4*B*). Additionally, these microglia were only weakly immune reactive to the activation marker, ED-1 (Fig. 4*C*). In contrast, microglia associated with noninvading lesions presented an amoeboid morphology with highly retracted processes (Fig. 4*E*), and were strongly ED-1 immune reactive (Fig. 4*F*). Interestingly, the edge of the noninvading tumor represented a line of demarcation, sharply dividing the ramified microglia outside from the activated microglia within (Fig. 4*D*). Because of the differences in the tumor ECM between invasive and noninvasive tumors, we hypothesized that tumor-associated CSPGs could be a factor responsible for mi-

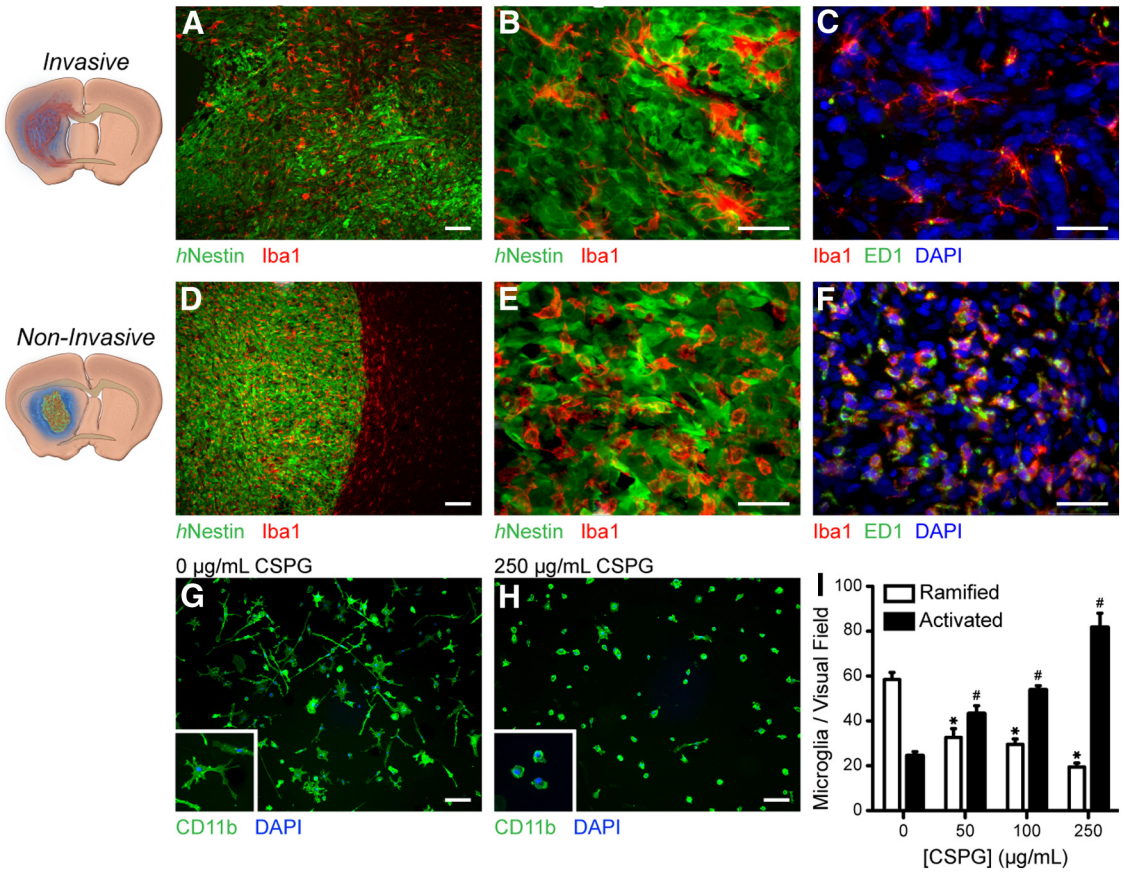

Figure 4. Microglial activation state differs markedly between invasive and noninvasive brain lesions. Representative low-magnification fluorescence micrographs demonstrate that microglia uniformly populate both (***A***) invasive and (***D***) noninvasive lesions. ***B***, An elaborate ramified morphology and (***C***) weak ED-1 immune reactivity characterize invasive tumor-associated microglia. In comparison, microglia confined within CSPG-rich noninvasive lesions demonstrate (***E***) the amoeboid morphology and (***F***) intense ED-1 immune reactivity indicative of a heightened state of activation and chronic inflammation. ***G***, inset, *In vitro*, in the absence of substrate-bound CSPGs, microglia maintain the ramified morphology indicative of the relatively decreased activation state observed in invasive tumor-associated microglia. ***H***, inset, In contrast, microglia exposed to increasing concentrations of CSPGs match the activated, amoeboid morphology indicative of heightened activation as seen in noninvasive tumors. ***I***, Quantification of microglial morphology demonstrates that CSPGs can serve as a potent activator of microglia (mean ± SEM, two-way ANOVA, Bonferroni-Dunn *post hoc* test, $*p < 0.0001$ as compared with 0, $\#p < 0.0001$ as compared with 0, $n = 30$/group). Scale bars: ***A–F***, 50 μm; ***G***, ***H***, 10 μm.

croglial activation within the noninvading lesions. We therefore tested whether CSPGs, by themselves, could induce such robust and uniform microglial activation. We challenged primary murine microglia with progressively increasing concentrations of substrate-bound CSPGs deposited evenly across an *in vitro* growth surface. Exposure to low concentrations of proteoglycans preserved the ramified morphology and weak ED-1 immune reactivity of resting microglia (Fig. 4*G*). However, with increasing levels of substrate-bound CSPGs, while the microglia remained bound to the CSPG-rich substrate (unlike astrocytes), they increasingly presented the amoeboid morphologies and concomitant ED-1 expression observed in the noninvasive tumors (Fig. 4*H*,*I*). To confirm that the cultured microglia were activated specifically by proteoglycans, and not by growing concentrations of substrate-bound protein, we replaced the CSPGs with escalating concentrations of BSA. BSA had no discernable activating effects on the microglia, even at the highest concentrations. Thus, because CSPGs alone were sufficient to induce the morphology and immune phenotype characteristic of activated microglia, the abundance of CSPGs within noninvading lesions, and relative absence from invasive lesions, may help explain the differential microglial response between these two distinct tumor types.

Reducing CSPG-mediated inhibition facilitates brain tumor invasion

The absence of glycosylated CSPGs from infiltrative brain tumors prompted the question of whether removal (or reduction) of CS-GAGs from the microenvironment of a noninvasive tumor could foster infiltration. *In vitro*, U-87MG cells grow initially as an even monolayer but coalesce into aggregates in the center of the growth surface above a critical density (Fig. 5*A*). We hypothesized that glycosylated CSPGs might mediate this self-aggregation *in vitro* and that this condensed growth might inform the self-contained growth of a U-87MG tumor *in vivo*. Therefore, we cultured U-87MG in the presence of progressively increasing concentrations of Ch'ase ABC. By removing the CS-GAGs, Ch'ase ABC has been shown to dramatically reduce the inhibitory properties of CSPGs (Silver and Miller, 2004; Crespo et al., 2007). In a dose-dependent manner, increasing concentrations of Ch'ase ABC resulted in the progressive decrease in the number of aggregates and a shift toward growth as an adherent monolayer (Fig. 5*B*,*C*), similar to its effects on cultured neurospheres (von Holst et al., 2006). Conversely, U-87MG aggregation was unaffected by the negative control, penicillinase–an alternative bacterial enzyme that has no biological substrate in the U-87MG culture system. Thus, our preliminary *in vitro* assessment suggested that the lengthy CS-GAG side

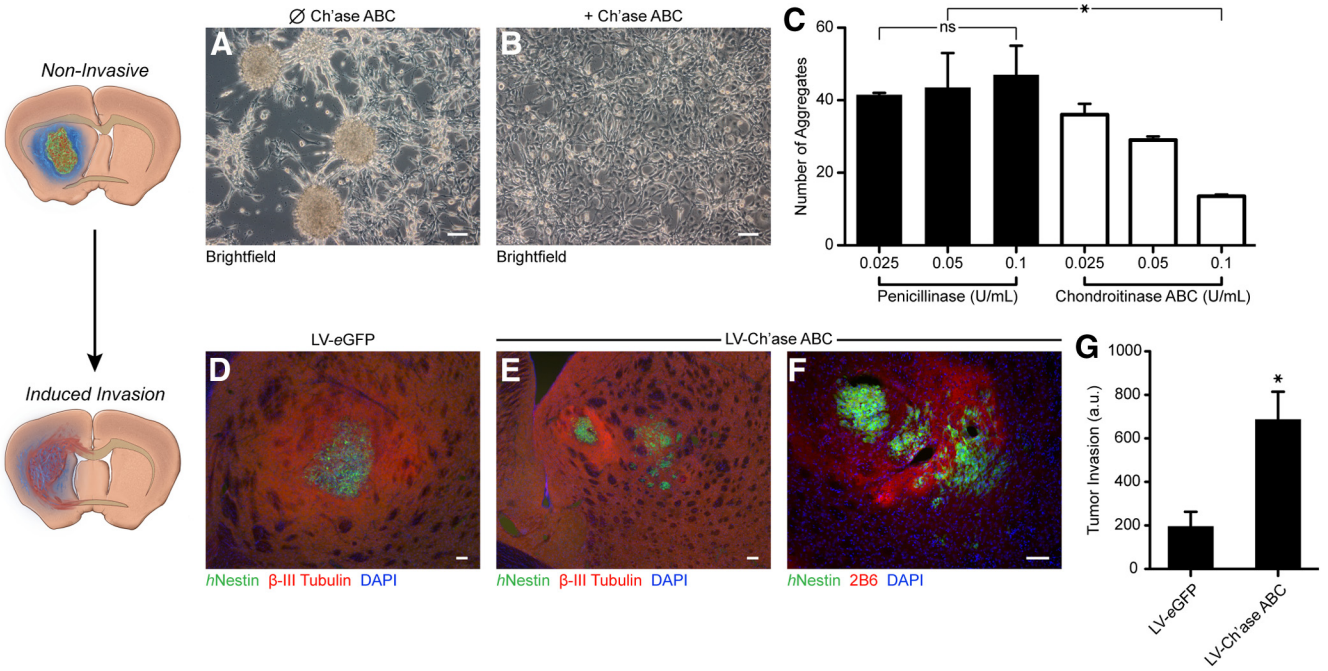

Figure 5. Reducing CS-GAG-mediated inhibition facilitates brain tumor invasion. ***A***, Tumor cell dispersal assays demonstrated that U-87MG aggregation is mediated through the potently inhibitory CS side chains that decorate the proteoglycan core proteins. ***B***, In a dose-dependent manner, addition of Ch'ase ABC, but not the negative control enzyme penicillinase, to the culture medium prevented aggregation and fostered the maintenance of an even monolayer of cells. ***C***, Quantification of the tumor cell dispersal assay emphasizes the effect of Ch'ase ABC on aggregate dispersal (mean ± SEM, one-way ANOVA, Newman–Keuls *post hoc* test, $*p < 0.05$, $n = 3$/group). ***D***, *In vivo*, while *e*GFP-expressing negative control cells present the noninvasive pathology typical of U-87MG, (***E***) induced Ch'ase ABC expression enables the diffuse infiltration of these formerly noninvasive tumor cells. ***F***, Immunostaining for 2B6 antibody confirmed that U-87MG infiltration occurred within zones of digested CS-GAGs. ***G***, Quantification of Ch'ase ABC-mediated invasion clarifies the inhibitory effects of CS-GAGs on tumor invasion. (a.u., arbitrary units; mean ± SEM, unpaired *t* test, $*p < 0.05$, $n = 7$ for LV-*e*GFP; $n = 15$ for LV-Ch'ase ABC). Scale bar, 10 μm.

chains either directly inhibit dispersal or, alternatively, might mediate a tight adhesion between tumor cells that is overcome by Ch'ase ABC treatment of the otherwise noninvasive cell line.

To test whether CSPGs also inhibit dispersal of noninvasive cells *in vivo*, we transduced U-87MG cells with lentiviral vectors encoding the genes for Ch'ase ABC (Jin et al., 2011) or *e*GFP. Consistent monolayer growth of the Ch'ase ABC-expressing cells, identical to the growth pattern depicted in (Fig. 5*B*), confirmed the activity of the enzyme, whereas the control *e*GFP-expressing cells grew into dense cellular aggregates, as seen in nontransduced or penicillinase-treated cells (Fig. 5*A*). Two separate cohorts of NOD/SCID animals received striatal transplants of either 50,000 U-87MG-Ch'ase ABC or U-87MG-*e*GFP cells ($n = 6$ each). *h*Nestin immunostaining then revealed that tumors derived from the *e*GFP-expressing cells developed as self-contained, noninfiltrating lesions across the entire rostral–caudal axis of the tumor (Fig. 5*D*). In contrast, the Ch'ase ABC-expressing cells did exhibit significant infiltration especially from the caudal aspect of the lesion (Fig. 5*E–G*); however, this diffuse pathology diminished toward the main body of the tumor. To confirm that this shift toward invasion was indeed caused by the de-glycosylation of CSPGs, we used the 2-B-6 antibody, which reveals sugar fragments left after Ch'ase ABC digestion. 2-B-6 immune reactivity confirmed that the Ch'ase ABC enzyme was active, specifically at sites where the induced invasion was most substantial (Fig. 5*F*). It is important to note that while 2-B-6 immune reactivity was present throughout the entire Ch'ase ABC-expressing tumor, CS-56 immune reactivity was notably reduced only at the caudal-most aspect of the tumor (data not shown). Thus, although regionally limited, where CS-GAG digestion was most successful, the resulting modified tumor microenvironment allowed for considerable tumor invasion.

Expression of the leukocyte common antigen-related phosphatase receptor distinguishes noninvasive from invasive brain lesions

CSPGs derived from noninvasive brain lesions remained highly abundant and concentrated within the tumor cell mass. In contrast, intrastriatal injection of soluble CSPGs (700 μg/ml in PBS) resulted in a relatively dim and widespread cloud of the protein, which, over time was diluted through extensive diffusion throughout the brain (data not shown). Recently, the leukocyte common antigen-related (LAR) family of protein tyrosine phosphatases (PTPRs) has been identified on neurons as functional receptors, which bind CS-GAGs at high affinity and help to explain the inhibitory actions of CSPGs in CNS injury (Shen et al., 2009; Fisher et al., 2011). We wondered whether noninfiltrating tumor cells might bind themselves directly to CS-GAGs through an active, receptor-mediated coupling. Using immunohistochemistry and Western blot analysis, we examined infiltrating and noninfiltrating tumors for the expression of the LAR phosphatase receptor (*PTPRF*). Interestingly, LAR was intensely expressed by noninvading lesions (Fig. 6*A*,*B*,*E*), and was entirely absent from diffusely infiltrating tumors (Fig. 6*C–E*). In noninvading lesions, expression of the receptor was perfectly coincident in space with the CSPG expression pattern. Throughout the entire noninvading tumor mass, the outer membrane of each tumor cell could be discerned by intense LAR immune reactivity. In the same way that the edge of the tumor precisely defined the space occupied by CSPGs, the edge of the tumor also set the outer limit for the expression of the LAR receptor. Additionally, of the other three recently described CSPG receptors, protein tyrosine phosphatase σ (PTPσ; Shen et al., 2009) was not detected and the nogo receptors, NgR1 and NgR3 (Dickendesher et al., 2012), were present in both tumor types at levels equivalent to the

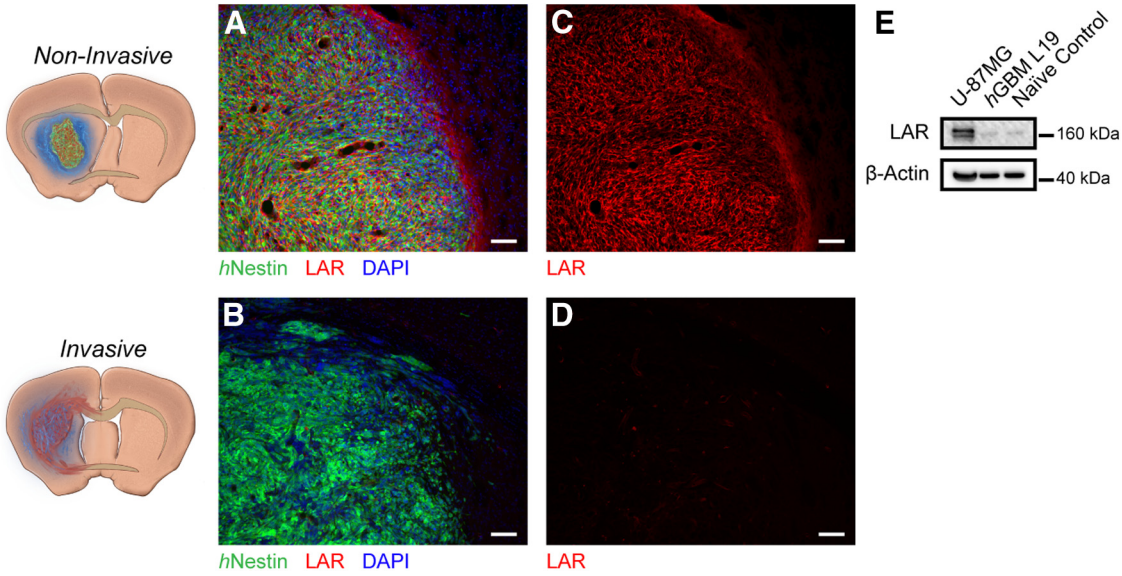

Figure 6. The CSPG receptor LAR differentiates invasive from noninvasive lesions. Representative fluorescence micrographs of (***A***) noninvasive and (***B***) invasive lesions highlight the disparity in the expression of the CS-GAG-binding, LAR phosphatase receptor. ***C***, Whereas LAR is uniformly expressed throughout the noninvasive tumor, (***D***) it is entirely absent from diffusely invasive lesions ($n = 6$/group). Scale bar, 50 μm. ***E***, Western analysis confirms the dichotomy in LAR expression between invasive and noninvasive tumors.

nontumor-bearing naive brain (data not shown). Thus, glycosylated CSPGs likely mediate a tight adhesion between the tumor cells and their ECM through LAR, which in turn may help to anchor CSPGs in place and resist passive diffusion.

Repelled by CS-GAGs, encapsulating reactive astrocytes may act as a secondary barrier to tumor invasion

Recall that CS-GAGs induce astrocytes to cluster around the circumference of spot cultures and that CS-GAG-rich noninvasive tumors induced a dense astrogliotic capsule (Fig. 3). Such astrogliotic scars are known to become physically obstructive over time, with a more rigid or leathery constitution than the surrounding brain tissue (Silver and Miller, 2004). We therefore hypothesized that the encapsulating reactive astrocytes, which are strongly repelled by glycosylated CSPGs, might be recruited as a secondary, physical barrier against the dissemination of tumor cells. We postulated that a reactive astrogliotic barrier could be used to constrain an otherwise invasive tumor cell population; however, our initial attempts, coinjecting invasive tumor cells within concentrated solutions of CSPGs, failed to generate an astrocyte barrier. Widespread diffusion of the proteoglycan likely prevented the establishment of a focal point away from which the astrocytes could withdraw (data not shown). We therefore reasoned that coengrafting invasive and noninvasive tumor cell lines could allow us to test whether the astrogliotic barrier generated by the CSPG-rich noninvasive cells could confine an invasive tumor cell population. To distinguish one cell line from the other, the invasive cell line *h*GBM L19 was transduced with a lentiviral vector encoding firefly luciferase (*h*GBM L19-*f*Luc) and the noninvasive line U-87MG was transduced to express *e*GFP (U-87MG-*e*GFP). It was also important that we account for any unforeseen differences in the proliferation rates of these separate tumor cell populations *in vivo*. Therefore, three separate cohorts of mice ($n = 3$ each) received intrastriatal transplants of 50,000 tumor cells comprised of the invasive line *h*GBM L19-*f*Luc mixed with the noninvasive U-87MG-*e*GFP. One cohort received equal parts invasive to noninvasive cells (1:1), the second cohort received double the number of invasive to noninvasive cells (2:1), and the third received half the number of invasive to noninvasive cells (1:2). Additionally, we allowed enough time (3 weeks post transplant) for an otherwise unencumbered *h*GBM L19-derived tumor to have displayed long-distance infiltration into the corpus callosum, approximately to the midline of the brain. In each case, a large, well defined astrocyte-enclosed mass occupied the majority of the striatum. The *f*Luc-expressing invasive cells organized into clusters or tendrils, swirling within the larger space-filling mass (Fig. 7*A*). These tendrils approached and, in some cases, skirted the edge of the larger mass; however, we did not observe any *f*Luc$^+$ invasive tumor cells escape the confines of the noninvasive lesion in any of our three groups. (Fig. 7*A*, dashed line). We also did not observe the induced expression of any of the CSPG receptors within the entrapped invasive cell population (data not shown). These findings suggested that the enveloping reactive astrocytes were not mere bystanders to this situation. Rather, the astrogliotic enclosure around the outer, noninvading mass may actually serve as a physical barrier, inhibiting the release of otherwise invasive tumor cells (Fig. 7*B*). Although intriguing, we were concerned that some other factor (or factors) within the U-87MG tumors had contributed to the confinement of the invasive tumor cells, potentially even at the edge of the noninvasive mass. As such, we adapted the *in vitro* spot assay to model the tumor/astrocyte interactions under both invasive and noninvasive conditions. Initially, by coculturing astrocytes and invasive *h*GBM L1 cells on Ch'ase ABC pretreated spots, we observed a uniform comingling of the two cell types–analogous to astrocyte/tumor interactions seen in invasive tumors ($n = 8 \times 4$ spots per cover glass; Fig. 7*C*,*E*). It is worth noting that while CS-GAGs are absent under these conditions, the CSPG core proteins are abundant and entirely permissive of the invasive phenotype. Alternatively, allowing astrocytes to first encapsulate, but not grow within, a heavily CS-glycosylated spot, we were able to generate an astrogliotic barrier in culture, which was capable of deflecting and containing invasive *h*GBM L1 cells to the astrocyte enclosed region ($n = 8 \times 4$ spots per cover glass; Fig. 7*D*,*E*). Thus, these findings suggest that the astrogliotic barrier, established as a result of the strong aversion of astrocytes to rich CS-GAG-containing environments, may be capable of constraining the movement of otherwise highly invasive tumor cell populations.

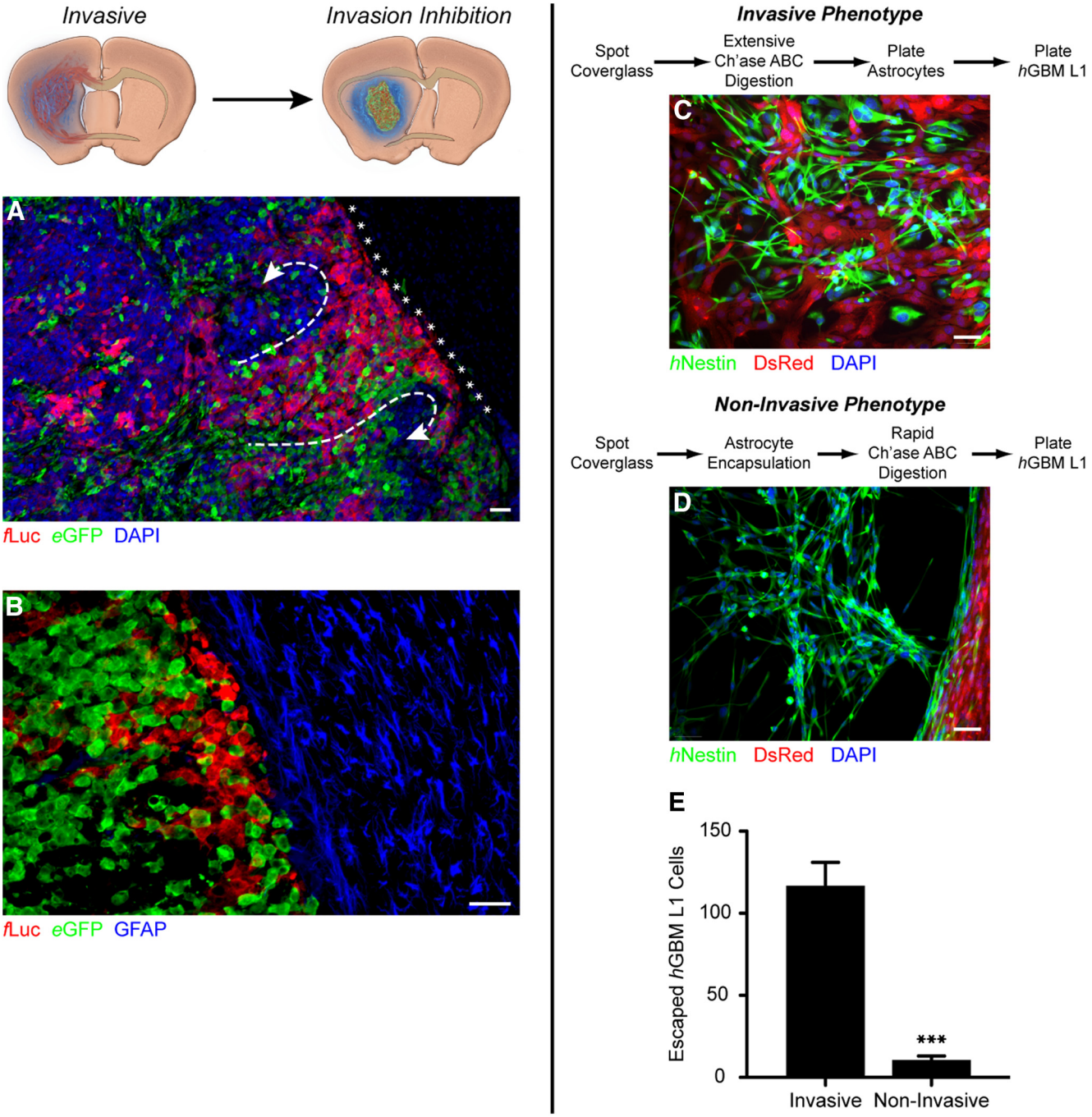

Figure 7. Cotransplantation of invasive and noninvasive tumors sequesters the invasive tumor within the boundaries on the noninvasive tumor mass. ***A***, A representative fluorescence micrograph of cotransplanted noninvasive U-87MG-*e*GFP (green) with invasive *h*GBM L19-*f*Luc (red) illustrates encapsulating astrocyte-mediated invasion inhibition. Invasive tumor cells (red), which organize into collective tendrils within the larger noninvasive mass, approach the edge of the lesion (asterisks) and are deflected in parallel to the (***B***) dense network of astrocyte fibers encapsulating the lesion ($n = 9$). Invasive and noninvasive tumor/astrocyte interactions can be modeled *in vitro* by manipulating the substrate and plating conditions of the spot assay. ***C***, Analogous to the invasive tumor phenotype, the absence of CS-GAGs permits tumor cells to insinuate themselves throughout an established astrocyte population. ***D***, In contrast, spots containing abundant CS-GAGs generated inhibitory astrogliotic barriers, capable of deflecting and containing otherwise invasive *h*GBM L1 cells ($n = 8$ cover glasses per group $\times$ 4 spots per cover glass). ***E***, Quantification of the invasive and noninvasive phenotype spot assays highlights the significant invasion inhibition achievable by highly patterned reactive astrocytes (mean $\pm$ SEM, unpaired *t* test, $^{***}p < 0.0001$). Scale bar, 50 μm.

Human clinical specimens verify that self-contained focused lesions, but not diffusely invasive brain tumors, are associated with the robust expression of CSPGs

It was critical that we validate our experimental findings with primary human tissue specimens. As such, we examined thin sections of paraffin-embedded samples of tumor-bearing tissue from neurosurgical resections using standard histology and immunohistochemistry. Parallel to our experimental findings, low-grade, benign pleomorphic xanthoastrocytoma (PXA; WHO grade II astrocytoma) presented clean borders (2 of 5; Fig. 8*A*) and abundant reactivity for the CSPG-specific antibody CS-56 (4 of 5; Fig. 8*B*). CSPG immune reactivity was distributed uniformly throughout the tumor mass, precisely defining the boundary of the PXA, and established a line of demarcation separating the benign tumor from the healthy adjacent brain tissue. Additionally, in accord with our experimental results, CSPG expression in

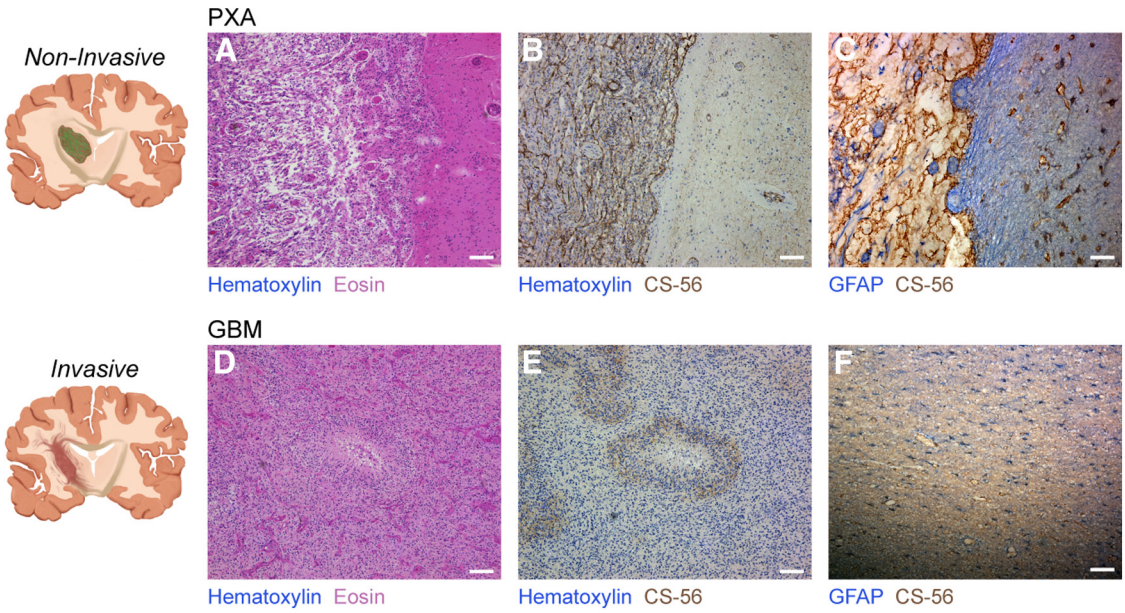

Figure 8. Human clinical specimens recapitulate the inverse relationship between abundant CS-GAGs and diffuse invasion. ***A***, Two of 5 PXA (grade II astrocytoma) specimens examined presented discrete lesions with well defined borders, while (***B***) 4 of 5 exhibited robust CS-GAGs expression. ***C***, Astrogliotic encapsulation was observed in 2 of 5 PXA specimens, in which the outer edge of the tumor was readily apparent. ***D***, In contrast, 5 of 5 highly infiltrative GBM specimens examined were (***E***) largely devoid of glycosylated CSPGs aside from minimal staining at sites of pseudopalisading necrosis. ***F***, Additionally, no obvious astrocyte patterning or encapsulation was noted, rather GFAP $^+$ reactive astrocytes were detected throughout the tumor samples, indicating the preservation of the astrocyte architecture.

5 of 5 high-grade, aggressively infiltrative GBM samples was negligible. We did observe some subtle CS-56 immune reactivity within pseudopalisading necrotic sites; however, this staining was likely nonspecific (Fig. 8*D*,*E*). Regardless, the intensity of the stain in the noninvasive PXAs far outstripped any questionable staining in the GBM samples. Identifying astrogliotic barriers in the noninvasive human tumor tissue was challenging, but could be identified in 2 of 5 PXAs (Fig. 8*C*). One must take into account the rarity of finding biopsy material that contains an edge of the tumor. Diagnostic biopsies, from which the majority of our archival human tissue was derived, are typically aimed at the core of lesions and thus, do not often extend to the outer boundaries of the tumor where astrogliotic encapsulation would be expected. Conversely, 5 of 5 human GBM samples presented the extensive comingling of tumor cells and resident reactive astrocytes characteristic of diffusely invasive lesions (Fig. 8*F*). In total, these data help to validate our experimental findings and reflect the relevance that the patient-derived human glioma cell lines have to the biology of brain tumor infiltration. Additionally, these data provide critical support for the novel concept that genuine glioma invasion occurs in the absence of a CS-GAG-rich inhibitory ECM.

Discussion

Our laboratory has developed a series of primary human GBM cell lines, which demonstrate long-distance infiltration throughout the brain after transplantation. The routes of invasion, referred to as the Secondary Structures of Scherer (i.e., perivascular satellitosis, subpial spread within and inferior to the meninges, and intrafascicular spread within patterned white matter tracts), reflect those observed in the human disease (Scherer, 1940). This study demonstrates for the first time that invasion of high-grade glioma occurs in the absence of a CS-GAG-rich inhibitory matrix. In contrast, discrete lesions that grow with defined edges–such as breast metastases to the brain (data not shown), certain low-grade gliomas, and many of the standard human glioma cell lines–are characterized by a robust, CS-GAG-containing ECM that both defines the mass and profoundly affects the stromal cells around and within the tumor. Our findings support the hypothesis that tumor-associated CSPGs are sufficient to induce the massive glial reorganizations that characterize the noninvasive tumor microenvironment and the absence of glycosylated CSPGs provides favorable conditions for the diffuse infiltration that typifies high-grade glioma (Fig. 9).

It is especially intriguing, in light of our results, that the presence rather than the absence of proteoglycans has been associated with gliomagenesis and invasion. Multiple groups have established causal links between glioma invasion and the expression of various CSPG core proteins. Significant overexpression of BCAN, NCAN, and VCAN have been well documented in primary human astrocytoma as compared with non-neural brain metastases and healthy controls (Jaworski et al., 1996; Varga et al., 2012). Interestingly, in agreement with our findings, when CS-glycosylation was assessed, investigators typically found that the pro-invasive effects were actually mediated by poorly glycosylated CSPG isoforms. For instance, the dominant tumor-associated isoform of BCAN, referred to as the hyaluronan-binding domain fragment (Zhang et al., 1998) or the B/b$_{\Delta g}$ isoform, was specifically identified as an "under-glycosylated" variant of BCAN (Viapiano et al., 2005). Similarly, glioma invasion has been attributed to the unglycosylated, soluble, short form of the phosphacan/RPTPζ molecule (Müller et al., 2003). The data on VCAN is less definitive. An invasion-promoting TGF-β2/VCAN interaction was described in one study, in which the characteristically smeared presentation of intact CSPGs on Western analysis suggested that the VCAN molecule was glycosylated. However, the extent of CS-glycosylation was not rigorously tested and the assessments of invasion were performed exclusively *in vitro* (Arslan et al., 2007). Because our findings demonstrate robust CS-glycosylation only under noninvasive con-

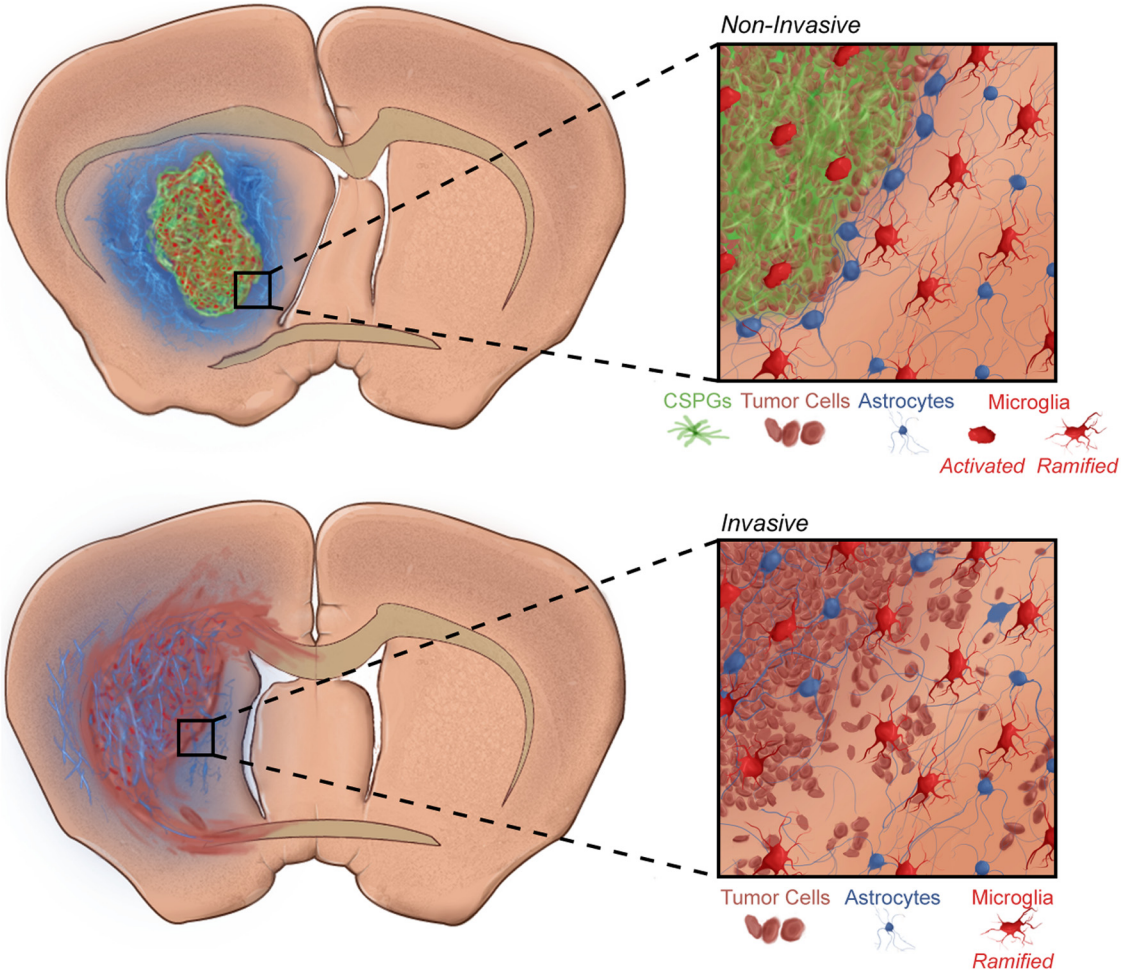

Figure 9. Putative model of CSPG-mediated invasion inhibition. CSPGs mediate both an intrinsic and extrinsic inhibition of tumor cell dissemination. When both receptor and ligand are expressed, tumor cells (brown) can bind themselves directly to glycosylated CSPG fibrils (green), intrinsically maintaining a dense and discrete mass. Additionally, abundant CS-GAGs induce dramatic spatial rearrangements in the peritumoral reactive astrocyte population (blue), which may serve as a secondary extrinsic inhibitor of tumor cell invasion. Microglia (red) are also induced into a heightened state of activation relative to their counterparts associated with invasive lesions. In the absence of both of these intrinsic and extrinsic blockades against tumor invasion, GBM tumor cells are free to disseminate widely throughout the brain parenchyma.

ditions *in vivo*, while readily detecting CSPG core proteins within invasive and noninvasive tumors (Fig. 2), we suggest that a synthesis of our results with the existing body of work helps to clarify that the opposing invasion inhibiting and promoting functions of CSPGs are mediated through their CS-GAG side chains. Further, our findings indicate the potential for future study of the molecular regulators of tumor cell CS-glycosylation, (i.e., the chondroitin sulfotransferases) as novel therapeutic targets.

Whether the tumor or the stromal astrocytes determine the final composition of the ECM remains elusive. For noninvasive tumors, it is clear that the heavily glycosylated, CSPG-rich microenvironment is primarily generated by the tumor cell population. Although extensive work has established that astrocytes also secrete CSPGs and other matrix molecules into the healthy and injured CNS (Yamada et al., 1997; Jones et al., 2003; Akita et al., 2008; Silver and Steindler, 2009; Schachtrup et al., 2010), the CS-GAG immune reactive noninvasive tumors were essentially devoid of reactive astrocytes (Fig. 3*A–B′*). In contrast, because of the substantial intermixing of reactive astrocytes and tumor cells within invasive tumors (Fig. 3*C–D′*), determining the primary source of the invasive tumor ECM is less clear and likely represents contributions from both the astrocyte and tumor cell populations. It is important to note that dot-blot analysis revealed a nominal quantity of glycosylated CSPGs within invasive tumors equal to that in the naive rodent brain (Fig. 2*G*). We therefore speculate that the glycosylated CSPG component of the invasive tumor ECM was produced by resident astrocytes, and was most likely culled from the innumerable perineuronal nets distributed throughout the invasive tumor-bearing hemisphere (Fig. 2*C′*,*D′*,*E′*). However, we cannot rule out the possibility that the abundant non-glycosylated (or weakly glycosylated) CSPG core proteins that precisely follow the contours of the invasive tumors may be derived directly from the tumor cell population.

Reactive astrocytes have been widely considered pro-invasive members of the tumor microenvironment and are thought to encourage the dispersal of glioma cells into the brain either through proteolysis of an initially present inhibitory ECM (Le et al., 2003) or the secretion of specific growth factors (Edwards et al., 2011). Our data suggest that the degree of CSPG glycosylation tunes the astrocyte response to the tumor resulting in two divergent modes of interaction: for noninvasive tumors, the densely entangled encapsulating astrocytes, repelled by the CS-GAG-rich tumor matrix, may actually contribute to the overall noninvasive phenotype by restricting tumor cell infiltration. In contrast, for CS-GAG-deplete invasive tumors, the more open, dispersed field of astrocytes permits or perhaps even facilitates tumor cell infil-

tration. While the concept of astrocyte-mediated invasion inhibition correlates with the function of astroglial barriers in the contexts of development and injury, the mechanism of this inhibition remains unknown. We hypothesize that the dense band of tightly interwoven processes that encapsulate noninvasive lesions (Fig. 3) may be capable of constraining invasive tumor cell populations by creating a physical obstruction to tumor cell movement (Fig. 7). Accordingly, reactive astrocyte enclosures around sites of traumatic brain or spinal cord injury provide a critical, putatively physical barrier, quelling inflammation and preventing wider spread of tissue damage (Windle and Chambers, 1950; Bush et al., 1999; Myer et al., 2006). Additionally, the molecular regulators that work in conjunction with physical obstruction in injury-associated astrogliotic barriers are likely also present within astrogliotic capsules surrounding noninvasive tumors. Thus, our data reveal greater complexity in the reactive astrocyte contribution to the tumor microenvironment. Modulated through the tumor ECM, this relationship is dynamic, allowing for both invasive and anti-invasive modes. Additionally, these findings hint at the possibility of using the tumor-confining abilities of reactive astrocytes therapeutically against tumor cell dissemination, a strategy that, to our knowledge, has not yet been explored.

Microglia are also typically considered facilitators of tumor cell dispersal (Charles et al., 2011). A causal link between the secretion of key microglial-derived proteases and tumor expansion has been firmly established (Markovic et al., 2009). Our data reaffirm this association, but also establish a potentially novel concurrence of microglia with noninvasive tumor growth. The activated (ED-1$^+$) but ramified microglia positioned immediately beyond the boundary of a noninvasive tumor (Fig. 4*D*) are highly reminiscent of injury-associated microglia. Because these microglia are know to play a critical role in cordoning off and inhibiting further spread of damage away from sites of CNS injury, we speculate that these tumor-adjacent microglia may likewise serve a noninfiltrative function (Nimmerjahn et al., 2005; Lalancette-Hébert et al., 2007; Rolls et al., 2008; Hines et al., 2009). Overall, our findings placed in context with the literature suggest that distinct microglial states, modulated through the ECM, may in turn result in pro- or anti-invasive contributions to the tumor microenvironment.

Developmentally, glycosylated CSPGs are not expressed as robustly or uniformly as in noninvasive brain tumors. Rather, these matrix molecules are positioned sparingly and strategically at the junctions of adjacent emerging structures (Cooper and Steindler, 1986; Steindler et al., 1988; Snow et al., 1990; Brittis et al., 1992; Jhaveri, 1993; Heyman et al., 1995; Golding et al., 1999). Further, proteoglycan boundaries typically repel or inhibit the movement of cells or processes away from restricted territories. Although the nature of CSPG repulsion is not clearly understood, it is striking that noninvasive tumor cells thrive within an environment awash in such abundant and heavily glycosylated CSPGs. The coincident expression of the CS-GAG receptor LAR (*PTPRF*) in the noninvasive tumor population may help explain the affinity of noninvasive tumor cells for this unique, potently inhibitory microenvironment. Recent work has demonstrated that LAR functions as an adhesive molecule, tethering cells to proteoglycans via their CS-GAG side chains (Lang et al., 2011). Thus, noninvasive tumor cells may be tightly held in place by a LAR-mediated coupling to the CS-GAG-rich ECM.

In total, we have presented the novel finding that the presence of heavily glycosylated, microenvironmental CSPGs inversely correlates with the invasive character of human glioma. This work presents a novel insight into the basic biology of the brain tumor microenvironment, the ECM, and their synergist influence over microscopic tumor cell invasion.

References

Akita K, von Holst A, Furukawa Y, Mikami T, Sugahara K, Faissner A (2008) Expression of multiple chondroitin/dermatan sulfotransferases in the neurogenic regions of the embryonic and adult central nervous system implies that complex chondroitin sulfates have a role in neural stem cell maintenance. Stem Cells 26:798–809. CrossRef Medline

Arslan F, Bosserhoff AK, Nickl-Jockschat T, Doerfelt A, Bogdahn U, Hau P (2007) The role of versican isoforms V0/V1 in glioma migration mediated by transforming growth factor-beta2. Br J Cancer 96:1560–1568. CrossRef Medline

Brittis PA, Canning DR, Silver J (1992) Chondroitin sulfate as a regulator of neuronal patterning in the retina. Science 255:733–736. CrossRef Medline

Bush TG, Puvanachandra N, Horner CH, Polito A, Ostenfeld T, Svendsen CN, Mucke L, Johnson MH, Sofroniew MV (1999) Leukocyte infiltration, neuronal degeneration, and neurite outgrowth after ablation of scar-forming, reactive astrocytes in adult transgenic mice. Neuron 23:297–308. CrossRef Medline

Charles NA, Holland EC, Gilbertson R, Glass R, Kettenmann H (2011) The brain tumor microenvironment. Glia 59:1169–1180. CrossRef Medline

Cooper NG, Steindler DA (1986) Lectins demarcate the barrel subfield in the somatosensory cortex of the early postnatal mouse. J Comp Neurol 249:157–169. CrossRef Medline

Crespo D, Asher RA, Lin R, Rhodes KE, Fawcett JW (2007) How does chondroitinase promote functional recovery in the damaged CNS? Exp Neurol 206:159–171. CrossRef Medline

DeAngelis LM (2001) Brain tumors. N Engl J Med 344:114–123. CrossRef Medline

Deleyrolle LP, Harding A, Cato K, Siebzehnrubl FA, Rahman M, Azari H, Olson S, Gabrielli B, Osborne G, Vescovi A, Reynolds BA (2011) Evidence for label-retaining tumour-initiating cells in human glioblastoma. Brain 134:1331–1343. CrossRef Medline

Dickendesher TL, Baldwin KT, Mironova YA, Koriyama Y, Raiker SJ, Askew KL, Wood A, Geoffroy CG, Zheng B, Liepmann CD, Katagiri Y, Benowitz LI, Geller HM, Giger RJ (2012) NgR1 and NgR3 are receptors for chondroitin sulfate proteoglycans. Nat Neurosci 15:703–712. CrossRef Medline

Edwards LA, Woolard K, Son MJ, Li A, Lee J, Ene C, Mantey SA, Maric D, Song H, Belova G, Jensen RT, Zhang W, Fine HA (2011) Effect of brain- and tumor-derived connective tissue growth factor on glioma invasion. J Natl Cancer Inst 103:1162–1178. CrossRef Medline

Faissner A, Steindler D (1995) Boundaries and inhibitory molecules in developing neural tissues. Glia 13:233–254. CrossRef Medline

Fisher D, Xing B, Dill J, Li H, Hoang HH, Zhao Z, Yang XL, Bachoo R, Cannon S, Longo FM, Sheng M, Silver J, Li S (2011) Leukocyte common antigen-related phosphatase is a functional receptor for chondroitin sulfate proteoglycan axon growth inhibitors. J Neurosci 31:14051–14066. CrossRef Medline

Furnari FB, Fenton T, Bachoo RM, Mukasa A, Stommel JM, Stegh A, Hahn WC, Ligon KL, Louis DN, Brennan C, Chin L, DePinho RA, Cavenee WK (2007) Malignant astrocytic glioma: genetics, biology, and paths to treatment. Genes Dev 21:2683–2710. CrossRef Medline

Galli R, Binda E, Orfanelli U, Cipelletti B, Gritti A, De Vitis S, Fiocco R, Foroni C, Dimeco F, Vescovi A (2004) Isolation and characterization of tumorigenic, stem-like neural precursors from human glioblastoma. Cancer Res 64:7011–7021. CrossRef Medline

Galtrey CM, Fawcett JW (2007) The role of chondroitin sulfate proteoglycans in regeneration and plasticity in the central nervous system. Brain Res Rev 54:1–18. CrossRef Medline

Gates MA, Thomas LB, Howard EM, Laywell ED, Sajin B, Faissner A, Götz B, Silver J, Steindler DA (1995) Cell and molecular analysis of the developing and adult mouse subventricular zone of the cerebral hemispheres. J Comp Neurol 361:249–266. CrossRef Medline

Golding JP, Tidcombe H, Tsoni S, Gassmann M (1999) Chondroitin sulphate-binding molecules may pattern central projections of sensory axons within the cranial mesenchyme of the developing mouse. Dev Biol 216:85–97. CrossRef Medline

Heyman I, Faissner A, Lumsden A (1995) Cell and matrix specialisations of rhombomere boundaries. Dev Dyn 204:301–315. CrossRef Medline

Hines DJ, Hines RM, Mulligan SJ, Macvicar BA (2009) Microglia processes block the spread of damage in the brain and require functional chloride channels. Glia 57:1610–1618. CrossRef Medline

Ito Y, Hikino M, Yajima Y, Mikami T, Sirko S, von Holst A, Faissner A, Fukui S, Sugahara K (2005) Structural characterization of the epitopes of the monoclonal antibodies 473HD, CS-56, and MO-225 specific for chondroitin sulfate D-type using the oligosaccharide library. Glycobiology 15: 593–603. Medline

Jaworski DM, Kelly GM, Piepmeier JM, Hockfield S (1996) BEHAB (brain enriched hyaluronan binding) is expressed in surgical samples of glioma and in intracranial grafts of invasive glioma cell lines. Cancer Res 56: 2293–2298. Medline

Jhaveri S (1993) Midline glia of the tectum: a barrier for developing retinal axons. Perspect Dev Neurobiol 1:237–243. Medline

Jin Y, Ketschek A, Jiang Z, Smith G, Fischer I (2011) Chondroitinase activity can be transduced by a lentiviral vector *in vitro* and *in vivo*. J Neurosci Methods 199:208–213. CrossRef Medline

Jones LL, Margolis RU, Tuszynski MH (2003) The chondroitin sulfate proteoglycans neurocan, brevican, phosphacan, and versican are differentially regulated following spinal cord injury. Exp Neurol 182:399–411. CrossRef Medline

Lalancette-Hébert M, Gowing G, Simard A, Weng YC, Kriz J (2007) Selective ablation of proliferating microglial cells exacerbates ischemic injury in the brain. J Neurosci 27:2596–2605. CrossRef Medline

Lang BT, Cregg JM, Weng YL, Li S, Silver J (2011) The LAR family of prosynaptic proteins help mediate glial scar induced axonal regeneration failure following spinal cord injury. Soc Neurosci Abstr 37:892.15.

Le DM, Besson A, Fogg DK, Choi KS, Waisman DM, Goodyer CG, Rewcastle B, Yong VW (2003) Exploitation of astrocytes by glioma cells to facilitate invasiveness: a mechanism involving matrix metalloproteinase-2 and the urokinase-type plasminogen activator-plasmin cascade. J Neurosci 23:4034–4043. Medline

Louis DN, Ohgaki H, Wiestler OD, Cavenee WK, Burger PC, Jouvet A, Scheithauer BW, Kleihues P (2007) The 2007 WHO classification of tumours of the central nervous system. Acta Neuropathol 114:97–109. CrossRef Medline

Markovic DS, Vinnakota K, Chirasani S, Synowitz M, Raguet H, Stock K, Sliwa M, Lehmann S, Kälin R, van Rooijen N, Holmbeck K, Heppner FL, Kiwit J, Matyash V, Lehnardt S, Kaminska B, Glass R, Kettenmann H (2009) Gliomas induce and exploit microglial MT1-MMP expression for tumor expansion. Proc Natl Acad Sci U S A 106:12530–12535. CrossRef Medline

Marshall GP 2nd, Demir M, Steindler DA, Laywell ED (2008) Subventricular zone microglia possess a unique capacity for massive in vitro expansion. Glia 56:1799–1808. CrossRef Medline

Müller S, Kunkel P, Lamszus K, Ulbricht U, Lorente GA, Nelson AM, von Schack D, Chin DJ, Lohr SC, Westphal M, Melcher T (2003) A role for receptor tyrosine phosphatase zeta in glioma cell migration. Oncogene 22:6661–6668. CrossRef Medline

Myer DJ, Gurkoff GG, Lee SM, Hovda DA, Sofroniew MV (2006) Essential protective roles of reactive astrocytes in traumatic brain injury. Brain 129:2761–2772. CrossRef Medline

Nimmerjahn A, Kirchhoff F, Helmchen F (2005) Resting microglial cells are highly dynamic surveillants of brain parenchyma in vivo. Science 308: 1314–1318. CrossRef Medline

Rolls A, Shechter R, London A, Segev Y, Jacob-Hirsch J, Amariglio N, Rechavi G, Schwartz M (2008) Two faces of chondroitin sulfate proteoglycan in spinal cord repair: a role in microglia/macrophage activation. PLoS Med 5:e171. CrossRef Medline

Sampetrean O, Saga I, Nakanishi M, Sugihara E, Fukaya R, Onishi N, Osuka S, Akahata M, Kai K, Sugimoto H, Hirao A, Saya H (2011) Invasion precedes tumor mass formation in a malignant brain tumor model of genetically modified neural stem cells. Neoplasia 13:784–791. Medline

Schachtrup C, Ryu JK, Helmrick MJ, Vagena E, Galanakis DK, Degen JL, Margolis RU, Akassoglou K (2010) Fibrinogen triggers astrocyte scar formation by promoting the availability of active TGF-beta after vascular damage. J Neurosci 30:5843–5854. CrossRef Medline

Scheffler B, Walton NM, Lin DD, Goetz AK, Enikolopov G, Roper SN, Steindler DA (2005) Phenotypic and functional characterization of adult brain neuropoiesis. Proc Natl Acad Sci U S A 102:9353–9358. CrossRef Medline

Scherer HJ (1940) A critical review: the pathology of cerebral gliomas. J Neurol Psychiatry 3:147–177. CrossRef Medline

Shen Y, Tenney AP, Busch SA, Horn KP, Cuascut FX, Liu K, He Z, Silver J, Flanagan JG (2009) PTPsigma is a receptor for chondroitin sulfate proteoglycan, an inhibitor of neural regeneration. Science 326:592–596. CrossRef Medline

Siebzehnrubl FA, Silver DJ, Tugertimur B, Deleyrolle LP, Siebzehnrubl D, Sarkisian MR, Devers KG, Yachnis AT, Kupper MD, Neal D, Nabilsi NH, Kladde MP, Suslov O, Brabletz S, Brabletz T, Reynolds BA, Steindler DA (2013) The ZEB1 pathway links glioblastoma initiation, invasion and chemoresistance. EMBO Mol Med 5:1196–1212. CrossRef Medline

Silver DJ, Steindler DA (2009) Common astrocytic programs during brain development, injury and cancer. Trends Neurosci 32:303–311. CrossRef Medline

Silver J, Miller JH (2004) Regeneration beyond the glial scar. Nat Rev Neurosci 5:146–156. CrossRef Medline

Snow DM, Steindler DA, Silver J (1990) Molecular and cellular characterization of the glial roof plate of the spinal cord and optic tectum: a possible role for a proteoglycan in the development of an axon barrier. Dev Biol 138:359–376. CrossRef Medline

Steindler DA, O'Brien TF, Cooper NG (1988) Glycoconjugate boundaries during early postnatal development of the neostriatal mosaic. J Comp Neurol 267:357–369. CrossRef Medline

Thomas LB, Gates MA, Steindler DA (1996) Young neurons from the adult subependymal zone proliferate and migrate along an astrocyte, extracellular matrix-rich pathway. Glia 17:1–14. CrossRef Medline

Tom VJ, Steinmetz MP, Miller JH, Doller CM, Silver J (2004) Studies on the development and behavior of the dystrophic growth cone, the hallmark of regeneration failure, in an in vitro model of the glial scar and after spinal cord injury. J Neurosci 24:6531–6539. CrossRef Medline

Varga I, Hutóczki G, Szemcsák CD, Zahuczky G, Tóth J, Adamecz Z, Kenyeres A, Bognár L, Hanzély Z, Klekner A (2012) Brevican, neurocan, tenascin-C and versican are mainly responsible for the invasiveness of low-grade astrocytoma. Pathol Oncol Res 18:413–420. CrossRef Medline

Viapiano MS, Bi WL, Piepmeier J, Hockfield S, Matthews RT (2005) Novel tumor-specific isoforms of BEHAB/brevican identified in human malignant gliomas. Cancer Res 65:6726–6733. CrossRef Medline

von Holst A, Sirko S, Faissner A (2006) The unique 473HD-Chondroitinsulfate epitope is expressed by radial glia and involved in neural precursor cell proliferation. J Neurosci 26:4082–4094. CrossRef Medline

Windle WF, Chambers WW (1950) Regeneration in the spinal cord of the cat and dog. J Comp Neurol 93:241–257. CrossRef Medline

Yamada H, Fredette B, Shitara K, Hagihara K, Miura R, Ranscht B, Stallcup WB, Yamaguchi Y (1997) The brain chondroitin sulfate proteoglycan brevican associates with astrocytes ensheathing cerebellar glomeruli and inhibits neurite outgrowth from granule neurons. J Neurosci 17:7784–7795. Medline

Zhang H, Kelly G, Zerillo C, Jaworski DM, Hockfield S (1998) Expression of a cleaved brain-specific extracellular matrix protein mediates glioma cell invasion *in vivo*. J Neurosci 18:2370–2376. Medline

Zheng PS, Wen J, Ang LC, Sheng W, Viloria-Petit A, Wang Y, Wu Y, Kerbel RS, Yang BB (2004) Versican/PG-M G3 domain promotes tumor growth and angiogenesis. FASEB J 18:754–756. Medline